Journal of Geophysical Research: Oceans

RESEARCH ARTICLE
10.1029/2018JC014312

Key Points:
- Resuspended sediments are an important contributor of the sinking particles collected by sediment traps, especially deep traps
- Provenance and seasonal variation of sinking particles can be identified by immobile-element discrimination diagrams
- The stable Nd isotopic composition coupled with conservative trace elements is a potential tool in provenance tracing

Supporting Information:
- Supporting Information S1
- Table S1
- Table S2

Correspondence to:
G. Wei,
gjwei@gig.ac.cn

Citation:
Liu, X., Wei, G., Zou, J., Guo, Y., Ma, J., Chen, X., et al. (2018). Elemental and Sr-Nd isotope geochemistry of sinking particles in the northern South China Sea: Implications for provenance and transportation. *Journal of Geophysical Research: Oceans*, *123*, 9137–9155. https://doi.org/10.1029/2018JC014312

Received 26 JUN 2018
Accepted 10 NOV 2018
Accepted article online 14 NOV 2018
Published online 15 DEC 2018

Elemental and Sr-Nd Isotope Geochemistry of Sinking Particles in the Northern South China Sea: Implications for Provenance and Transportation

Xi Liu[1,2], Gangjian Wei[1], Jieqiong Zou[1,2], Yangrui Guo[1,2], Jinlong Ma[1], Xuefei Chen[1,2], Ying Liu[1], Jianfang Chen[3], Hongliang Li[3], and Ti Zeng[4]

[1]State Key Laboratory of Isotope Geochemistry, Guangzhou Institute of Geochemistry, Chinese Academy of Sciences, Guangzhou, China, [2]College of Earth and Planetary Sciences, University of Chinese Academy of Sciences, Beijing, China, [3]SOA, The Second Institute of Oceanography, Hangzhou, China, [4]CAS Key Laboratory of Marginal Sea Geology, Guangzhou Institute of Geochemistry, Chinese Academy of Sciences, Guangzhou, China

Abstract Major and trace elements, Sr and Nd isotopes of bulk particles from the SCS-NW and SCS-N-03 traps were studied to trace the provenance of sinking particles in the northern South China Sea (SCS). About 63% of biogenic materials and most of lithogenic materials from the SCS-NW trap may be contributed from resuspended sediments, and more biogenic materials are collected in winter than in summer. The immobile-element discrimination diagrams also indicate that the lithogenic materials of particles are, to a large degree, from local seafloor sediments, and that the lithogenic materials of particles from SCS-N and SCS-W traps have seasonal variations. Sr isotopes ($^{87}Sr/^{86}Sr$ and $\delta^{88}Sr$) of bulk particles are significantly influenced by biogenic materials and cannot be used in provenance tracing. In contrast, Nd isotopes are ideal tools to trace particle provenance. However, the traditional Nd isotope ($^{143}Nd/^{144}Nd$) shows no statistical difference on the particles of the SCS-NW and SCS-N-03 traps, making it unable to identify their provenance. Fortunately, the stable Nd isotope, $\varepsilon^{146}Nd$, shows different correlation trends to $\varepsilon^{143}Nd$ in these two traps, suggesting that stable Nd isotope can potentially identify the sources of lithogenic materials in the northern SCS. Our results indicate that distribution and transportation of sinking particles are controlled by currents of the SCS mainly driven by the East Asian Monsoon.

Plain Language Summary As the largest semi-enclosed marginal sea in the west Pacific, the South China Sea (SCS) is supplied with a large amount of suspended sediments from its surrounding continents and islands. Studies on sedimentary process and source of sediments in the SCS have long been carried out, but no consensus has been reached yet. This study presents elemental and Sr-Nd isotope geochemistry of sinking particles from the northern SCS. According to fluxes and element concentrations of sinking particles, we find that resuspended sediments are an important contributor to sinking particles in the SCS. The relationship between trace elements of sinking particles and offshore surface sediments indicates that these resuspended sediments may be derived from continental shelves. The distribution and transportation of sinking particles are influenced by hydrological conditions of the SCS mainly driven by the East Asian monsoon. This study also reveals that stable Nd isotope could be a powerful tool in tracing sediment provenances in the northern SCS. Therefore, our results will improve the understanding of sediment transportation and sedimentary processes in the northern SCS.

1. Introduction

Sediment traps at various water depths collect particles directly sinking through the water column and provide important information on fluxes of biogenic materials and terrestrial inputs that are helpful for understanding modern biological and sedimentary processes. Given that biogenic materials are the main components of sinking particles in open oceans, sediment traps have long been used to trace particle fluxes linked to surface productivity (Buesseler et al., 2007; Hwang et al., 2017; Yan et al., 2007). In regions close to continental margin, such as marginal seas, fluvial sediments or eolian dusts also significantly contribute to sinking particles. In this respect, particles collected by sediment traps may also be used in tracing terrestrial inputs that may advance our understanding of transportation process of sediments (J. G. Liu et al., 2014; Schröder et al., 2015).

The South China Sea (SCS) is the largest marginal sea in the west Pacific. Terrestrial materials transported to the SCS are supplied from the surrounding continents and islands. A number of efforts have been made to trace the provenance of sediments in the SCS using multiple proxies, such as detrital mineral assemblages (Z. F. Liu et al., 2010, 2008; Yan et al., 2007) and elemental and isotopic geochemistry (Li et al., 2003; Z. F. Liu et al., 2008; Shao et al., 2009; Wei et al., 2012). However, no consensus has been reached. For example, in the northern SCS, where terrestrial detritus is transported mainly from adjacent continents (e.g., South China) and islands (e.g., Taiwan and Hainan Islands), data on clay assemblages suggest that both South China and Taiwan Island significantly contribute to the fine components of sediments in this region (Z. F. Liu et al., 2010, 2008; J. G. Liu et al., 2014). However, the geochemistry of surface sediments suggests that sediments in the western part of the northern SCS (west of the Pearl River mouth) are imported mainly from western South China, whereas those in the region east of the Pearl River mouth are derived mainly from eastern South China (ESC, including Taiwan Island) (Wei et al., 2012). These studies were all based on research on surface sediments in the SCS. If additional information from sediment traps were to be used, together with data from modern sediment transportation, the provenance of sediments in this region could be elucidated more clearly.

Sediment trap experiments have been carried out in the SCS for years, but previous studies mainly considered the flux of biogenic materials (Chen et al., 1998; Chung et al., 2004; Lahajnar et al., 2007). Some recent works have focused on the clay mineral assemblages of the collected particles, with the aim of tracing their provenance (J. G. Liu et al., 2014; Schröder et al., 2015). No seasonal change has been observed in the clay mineral assemblages of the particles collected by the XI sediment trap in the Xisha Trough (J. G. Liu et al., 2014), suggesting a steady input pattern for clay minerals in this region. Schröder et al. (2015) analyzed data from sediment traps in the SCS and reported that clay minerals sinking to the shallow traps are probably controlled by surface currents. However, particles collected by deep traps are less variable and display increasing smectite content with water depth, which indicates complicated transportation processes including lateral advection and resuspension of shelf sediments (Schröder et al., 2015); other factors such as authigenic smectite may also be relevant.

In addition to clay mineral assemblages, the geochemical components of bulk sediments are common and powerful tools in provenance analysis. Schröder (2015) analyzed trace elements of the bulk particles ($<$1 mm) collected by sediment traps in the SCS and concluded that Eu anomaly, LREE/HREE (light rare earth elements/heavy rare earth elements), and Zr/Sc ratios are more reliable than clay mineral assemblages in source identification. Trace element concentrations become higher with increasing water depths, which also implies enrichment of resuspended detrital sediments in deep ocean (Schröder, 2015). Although Nd isotopes of sinking particles have rarely been analyzed, Nd isotopes have served as reliable tracers of provenance analysis because their compositions are stable during diagenesis and transport (Goldstein et al., 1984; Goldstein & Jacobsen, 1988; Li et al., 2003; Shao et al., 2009). Associated with Nd isotopes, Sr isotopes are also useful in tracing the provenance of marine sediments (Goldstein & Hemming, 2003; Jiang et al., 2016; Wei et al., 2012). Therefore, the Sr-Nd isotope characteristics of sinking particles may also be effective signals in provenance analysis.

Previous works usually analyze the provenance of sinking particles by comparing them with fluvial sediments (J. G. Liu et al., 2014; Z. F. Liu et al., 2016; Schröder, 2015; Schröder et al., 2015). However, most of fluvial sediments deposit on the estuary and continental shelf and could not be transported directly to the open sea. For example, only 1–15% of the sediments from the Yellow River could pass through the shelf edge and be transported to Yellow Sea (Alexander et al., 1991; Martin et al., 1993; Qiao et al., 2017), and the fine-grained sediments from the Mekong River are barely be exported into the deep basin of the SCS (Szczucinski et al., 2013). In other words, fluvial sediments are the initial materials transported into the SCS but possibly not the direct materials collected by sediment traps. Resuspended sediments from the continental shelf were often regarded as a potential contributor for sinking particles (J. G. Liu et al., 2014; Schröder, 2015), and they may also be the source of sinking particles collected by traps far from the shelf.

Herein we analyze the major and trace elements, and Sr and Nd isotopes of the time series of bulk particles collected by the SCS-NW and SCS-N-03 sediment traps in the northern SCS. Combined with trace elements of sinking particles and offshore surface sediments from previous works, we attempt to identify the particle provenance using multiple geochemical proxies. It shows that discrimination of immobile elements and stable

Nd isotopes, a novel new isotope tool, can effectively identify the provenance of the sinking particles in the northern SCS. The new evidence provided in this work will improve our understanding of particle transportation and sedimentary processes in the northern SCS.

2. Regional Background

As the largest semi-enclosed marginal sea in the west Pacific, the SCS is surrounded by South China in the north, the Indochina Peninsula in the west, Malay Peninsula and Sumatra in the southwest, Borneo and Palawan in the south, Luzon in the east, and Taiwan in the northeast. The suspended sediments of about 700–1,600 million tons, the largest fluvial sediment discharge into marginal sea in the world, are annually supplied to the SCS by rivers on these lands, and southwest Taiwan, South China, and eastern Indochina Peninsula largely contribute suspended sediments of 416 Mt/year to the northern SCS (Z. F. Liu et al., 2016). Sediments derived from South China (102 Mt/year) or the Pearl River (80 Mt/year) generally move southwestward and deposit along continental shelf (J. G. Liu et al., 2011, 2013; Milliman & Farnsworth, 2013). As a main sediment discharger from eastern Indochina Peninsula, the Red River mostly transport sediments of 110–130 Mt/year into the Beibuwan Bay (Gulf of Tonkin, Milliman & Farnsworth, 2013; Milliman & Syvitski, 1992). Furthermore, the mountainous rivers on southwest Taiwan can contribute 176 Mt/year of sediments to the SCS (Z. F. Liu et al., 2016), which are mainly carried into the northeast SCS slope (J. G. Liu et al., 2011, 2013). Eolian dust is another contributor of detrital matter in the SCS and should be considered. Based on end-member modeling of the grain size data, Boulay et al. (2007) concluded that 5.5–11% of the terrigenous fractions at Ocean Drilling Program Site 1146 were supplied by eolian dust during the Pleistocene. However, eolian supply is a very minor component of modern sediments for the SCS. Annual fluxes of fluvial sediments into the SCS are 700–1,600 Mt/year, but annual fluxes of eolian dust may be only 4.5–11.5 Mt/year (Schröder, 2015; S. H. Wang et al., 2012). Therefore, the contribution of eolian dust to sinking particles in the SCS can be negligible.

The SCS is influenced by the East Asian monsoon system. In winter, strong northeasterly monsoon develop from November to March of the next year; southwesterly summer monsoon prevail from May to September; the rest of other months are transitional periods, and different wind directions may exist together in the SCS (Huang et al., 1994; Shaw & Chao, 1994). Semi-enclosed topography of the SCS make the surface water mass sensitive to monsoon reversal. Consequently, the circulation patterns in the SCS have similar seasonal reversal. Driven by the East Asian monsoon, the surface layer (0–500 m) circulations of the SCS are cyclonic in the winter and anticyclonic in the summer; in the intermediate layer (500–1,500 m), the compensatory movements of water mass produce an anticyclonic circulation in the winter and a cyclonic circulation in the summer (Figure 1, Fang et al., 1998; Huang et al., 1994; Zhu et al., 2016). Another significant factor affecting the northern SCS circulations is the Kuroshio intrusion current. The Kuroshio intrudes into the SCS through the Luzon Strait in winter, and the intrusion move westward on the northern continental slope of the SCS (Fang et al., 1998; Hu et al., 2000; Shaw & Chao, 1994). However, the existence of the intrusion in the summer is still a matter of debate (Fang et al., 1998; Hu et al., 2000; Shaw & Chao, 1994).

3. Materials and Methods

3.1. Sediment Traps

Two Mark VI (McLane, USA) time series sediment traps with a collection area of 0.5 m^2 have been set in the northern SCS. The first trap, SCS-NW, is set at 110°40.2′E, 17°25.8′N at a water depth of 1,548 m. This trap is very close to the XS1 sediment trap (110°55.0′E, 17°24.5′N) of the South China Sea Institute of Oceanology, Chinese Academy of Sciences (J. G. Liu et al., 2014). The second trap, SCS-N-03, is set at 116°1.8′E, 18°27.6′N at a water depth of 1,000 m (Figure 1). A standard sampling procedure is followed (Lahajnar et al., 2007; Li et al., 2017). Prior to deployment, the sample bottles were filled with filtered seawater from trap-deployed depths. Analytical grade NaCl (35 g/L) and $HgCl_2$ (3.3 g/L) were added into each sample bottle to minimize diffusive processes and inhibit microbial activity. Samples were recovered from each trap at intervals of 15–30 days. After recovery, the wet samples were emptied from bottles into a 1-mm mesh nylon sieve to exclude zooplankton. The <1 mm fractions were split into aliquots by a high-precision rotary splitter (McLane WSD-10) and filtered on preweighed polycarbonate filters with 0.45-μm pore size. Subsequently, the samples was first dried and weighed to calculate the total particle flux (TPF) prior to separation for

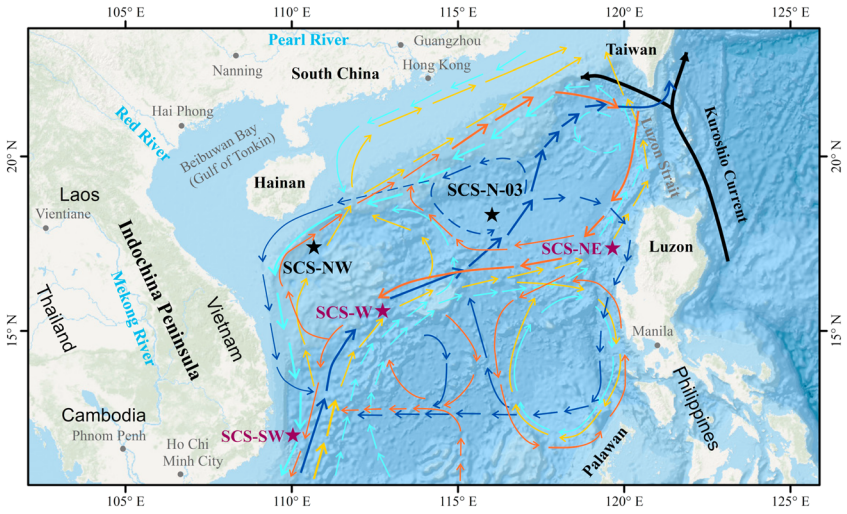

Figure 1. Sediment trap locations and current patterns in the northern South China Sea. Black and purple stars are sampling locations of this article and Schröder et al. (2015), respectively. The surface and intermediate currents are basically depicted by Zhu et al. (2016) and Hu et al. (2000): The surface currents are indicated by light blue arrows (winter) and yellow arrows (summer); the intermediate currents are indicated by dark blue arrows (winter) and orange arrows (summer). The Kuroshio Current is indicated by the black arrows (Fang et al., 1998).

multiple analyses. The samples obtained between July 2012 and April 2013 in the SCS-NW sediment trap and from March to April 2010 in the SCS-N-03 sediment trap were used in this study. Unlike seafloor surface sediments and sediment cores, only limited samples could be captured by sediment trap so that an aliquot of 20–50 mg of the bulk particles of each sample was separated for geochemical analysis.

3.2. Geochemical Analysis

The bulk particles were first ground into powder and then digested using an HNO_3 + HF acid mixture. The solution of each sample was separated into three parts for major element, trace element, and Sr-Nd isotope measurements. All the chemical treatments and instrument analyses were carried out at the State Key Laboratory of Isotope Geochemistry (SKLIG) in the Guangzhou Institute of Geochemistry, Chinese Academy of Sciences (GIG-CAS), Guangzhou, China.

Major elements were measured using a Varian Vista Pro inductively coupled plasma atomic emission spectrometry (ICP-AES), and trace elements were measured with a Thermo ICAP Qc inductively coupled plasma mass spectrometry (ICP-MS). Analytical details for major- and trace-element measurements are described by Li et al. (2002) and Y. Liu et al. (1996), respectively. The precision for measurements of major elements was better than 1% (Li et al., 2002) and was generally better than 5% (relative standard deviation) for trace elements (Y. Liu et al., 1996). The results of the analyses are presented in Table 1 (major elements) and Table 2 (trace elements). Several United States Geological Survey and Chinese soil and sediment standard references, such as GSS-5, GSS-7, and GXR-6 (soils), and GSD-9 and GSD-12 (sediments), were chemically treated and measured with the samples to monitor the quality of the major- and trace-element measurements. The results were generally within the range of ±10% (relative standard deviation) of the certified values.

The aliquot for Sr and Nd isotope measurement was dried on a hot plate and redissolved in 4 mol/L HNO_3 solution for further Sr and Nd purification. The solution was first loaded on an ion chromatograph comprising an Eichrom polypropylene column filled with Eichrom-Sr-Resin, which is generally used for Sr purification. Sr was trapped on the column, and the elution was collected for further Nd purification. The trapped Sr was eluted using 8-mL Milli-Q water and further diluted to achieve a Sr concentration of ~50 ng/mL for instrumental measurement. Further details of the Sr purification method are provided by Ma et al. (2013a).

The eluant from the Sr column was dried again and redissolved with 2 mL of 6 M HCl for 4 hr capped on a hot plate. The solution was dried again and finally redissolved with 1 mL 2.5 M HCl for Nd purification. Nd purification was performed using a two-column ion-exchange chromatography procedure. The first column

Table 1
Total Particle Flux and Major Elements of the Sinking Particles Collected by the SCS-NW and SCS-N-03 Traps

Sample ID	Sampling duration (yyyy/mm/dd)	Total particle flux (mg/m^2/day)	Al_2O_3 (wt %)	CaO (wt %)	Fe_2O_3 (wt %)	K_2O (wt %)	MgO (wt %)	MnO (wt %)	Na_2O (wt %)	P_2O_5 (wt %)	TiO_2 (wt %)
Trap: SCS-NW: 110°40.2′E, 17°25.8′N											
SCS-NW-1	2012/7/22 to 8/6	861	18.27	13.26	5.64	2.82	3.01	0.14	5.30	0.22	0.69
SCS-NW-2	2012/8/6 to 8/21	1271	12.22	7.88	4.37	2.06	2.08	0.12	2.52	0.13	0.58
SCS-NW-3	2012/8/21 to 9/5	383	13.95	8.39	4.98	2.38	2.26	0.16	3.00	0.15	0.61
SCS-NW-4	2012/9/5 to 9/20	120	10.00	11.85	3.59	1.70	1.94	0.12	3.94	0.19	0.43
SCS-NW-5	2012/9/20 to 10/5	208	11.67	11.00	4.20	1.98	2.10	0.14	3.39	0.20	0.51
SCS-NW-6	2012/10/5 to 10/20	1228	12.30	8.91	4.49	2.17	2.06	0.11	2.23	0.18	0.60
SCS-NW-7	2012/10/20 to 11/4	1084	12.52	9.67	4.58	2.26	2.11	0.11	2.28	0.21	0.62
SCS-NW-8	2012/11/4 to 11/19	297	11.55	11.74	4.21	2.07	2.08	0.11	2.64	0.16	0.57
SCS-NW-9	2012/11/19 to 12/4	148	9.17	14.47	3.33	1.54	1.87	0.10	3.09	0.16	0.42
SCS-NW-10	2012/12/4 to 2013/1/3	332	8.32	16.75	3.01	1.43	1.65	0.10	2.64	0.16	0.39
SCS-NW-11	2013/1/3 to 2/2	1094	10.29	12.87	3.67	1.85	1.84	0.09	2.69	0.16	0.46
SCS-NW-12	2013/2/2 to 3/4	2500	14.68	8.02	5.24	2.54	2.27	0.13	2.35	0.14	0.69
SCS-NW-13	2013/3/4 to 3/19	243	10.75	12.77	3.89	1.94	1.94	0.12	2.60	0.15	0.49
SCS-NW-14	2013/3/19 to 4/3	300	10.48	12.34	3.74	1.83	1.93	0.10	2.88	0.17	0.44
SCS-NW-15	2013/4/3 to 4/18	279	8.89	15.89	3.24	1.66	1.83	0.10	3.52	0.18	0.40
SCS-NW-16	2013/4/18 to 4/21	260	7.89	14.21	5.84	1.49	1.70	0.10	3.59	0.16	0.37
Trap: SCS-N-03: 116°1.8′E, 18°27.6′N											
SCS-N-03-1	2010/3/10 to 3/26		6.76	20.02	2.65	1.09	1.11	0.12	1.75	0.17	0.28
SCS-N-03-2	2010/3/26 to 4/11		10.73	15.29	3.94	2.03	1.51	0.12	1.40	0.17	0.45
SCS-N-03-3	2010/4/11 to 4/27		7.83	15.16	2.99	1.37	1.28	0.10	1.36	0.14	0.34

was filled with AG50W-x12 strong cation resin (Bio-Rad Company) to preconcentrate rare earth elements (REEs), and the second column was filled with Ln resin with di (2-ethylhexyl) orthophosphoric acid (HDEHP; Eichrom Company) to separate Nd from other REEs. The purified Nd was eluted using 0.25-M HCl and dried on a hot plate. Subsequently, 0.5 mL of concentrated HNO_3 was added, dried again, and finally redissolved in 2% HNO_3 for mass spectrometry measurement. Further details of the Nd purification method are provided by Ma et al. (2013b).

Both Sr and Nd isotopes were measured on a Thermo Fisher Scientific Neptune Plus multicollector-inductively coupled plasma-mass spectrometer (MC-ICP-MS) of the State Key Laboratory of Isotope Geochemistry at GIG-CAS. In addition to the traditional radiogenic Sr and Nd isotopes ($^{87}Sr/^{86}Sr$ and $^{143}Nd/^{144}Nd$), the stable Sr isotope, defined as $\delta^{88}Sr = (^{88}Sr/^{86}Sr_{sample}/^{88}Sr/^{86}Sr_{SRM987}-1) \times 1000$, and the stable Nd isotope, defined as $\varepsilon^{146}Nd = (^{146}Nd/^{144}Nd_{sample}/^{146}Nd/^{144}Nd_{JNdi\text{-}1} - 1) \times 10{,}000$, were measured at the same time. Sr isotope measurements were carried out using standard sample bracketing mode in the sequence SRM 987-sample-SRM 987, in accordance with the method of Ma et al. (2013a). To eliminate short-term instrument drift, Zr was added to each sample and standard solution before measurement, and

Journal of Geophysical Research: Oceans

10.1029/2018JC014312

Table 2
Trace Elements of the Sinking Particles Collected by the SCS-NW and SCS-N-03 Traps

Sample ID	SCS-NW-1	SCS-NW-2	SCS-NW-3	SCS-NW-4	SCS-NW-5	SCS-NW-6	SCS-NW-7	SCS-NW-8	SCS-NW-9	SCS-NW 10	SCS-NW 11	SCS-NW 12	SCS-NW 13	SCS-NW 14	SCS-NW 15	SCS-NW 16	SCS-N-03-1	SCS-N-03-2	SCS-N-03-3
Li (ppm)	70.4	53.7	61.6	45.9	50.9	53.9	55.1	50.2	41.7	38.6	47.7	64.4	48.5	47.2	38.2	33.6	22.1	34.7	28.3
Be (ppm)	2.47	1.93	2.23	1.73	1.80	1.97	2.19	1.94	1.54	1.37	1.76	2.25	1.74	1.59	1.43	1.27	0.94	1.61	1.21
P (ppm)	1,019	640	731	860	889	798	984	688	766	731	702	705	752	769	819	772	792	805	696
Sc (ppm)	16.0	10.8	12.3	9.07	10.4	11.2	11.3	10.4	8.83	8.17	9.55	13.2	10.3	9.68	8.99	8.07	7.99	10.9	8.44
Ti (ppm)	3,972	3,331	3,502	2,425	2,834	3,421	3,620	3,251	2,467	2,258	2,682	3,860	2,908	2,552	2,345	2,146	1,524	2,573	1,973
V (ppm)	96.6	77.5	88.9	65.7	75.0	79.6	82.7	75.7	62.8	58.8	67.7	93.6	74.1	69.3	66.7	67.2	56.0	78.1	61.7
Cr (ppm)	69.7	52.2	59.4	44.4	50.2	55.3	58.2	57.2	46.5	45.2	46.8	63.0	53.3	50.6	47.5	66.5	36.5	50.8	41.7
Mn (ppm)	1056	889	1147	880	1003	833	847	809	771	748	697	964	878	755	748	719	879	853	746
Co (ppm)	14.1	11.5	13.6	10.4	11.6	11.4	11.9	11.2	10.0	9.5	10.1	13.5	11.6	10.7	10.3	10.4	9.8	12.7	9.8
Ni (ppm)	45.2	34.7	40.1	34.2	36.6	33.7	35.4	42.0	34.0	34.8	33.8	39.2	37.5	34.8	38.1	43.2	34.7	35.7	35.7
Cu (ppm)	39.5	25.7	37.3	36.2	144.1	25.4	41.1	36.3	25.3	28.0	26.1	28.3	31.7	28.2	31.1	205	47.2	36.4	37.8
Zn (ppm)	138	101	138	111	130	131	118	125	98	92	92	118	114	96	115	522	168	116	121
Ga (ppm)	20.9	15.9	18.2	12.7	15.1	16.1	16.4	14.8	12.1	11.2	13.7	19.2	14.5	13.6	11.7	10.7	8.6	13.4	10.1
Ge (ppm)	1.39	1.01	1.06	0.81	0.91	0.99	1.09	0.94	0.80	0.71	0.86	1.15	0.90	0.85	0.73	1.07	0.62	0.82	0.69
Rb (ppm)	135	101	118	71.8	86.8	103	107	87.3	58.3	55.7	82.8	125	85.6	76.0	63.0	56.6	46.2	84.5	61.0
Sr (ppm)	474	323	340	414	395	345	386	444	557	619	496	343	511	491	641	537	697	554	594
Y (ppm)	29.6	20.1	20.0	14.6	16.7	20.0	20.9	19.6	15.6	14.6	16.1	22.7	18.0	15.6	15.1	14.3	10.6	14.9	12.6
Zr (ppm)	117	97.7	94.4	66.5	78.0	104	113	100	74.2	70.3	76.0	111	85.0	73.6	70.4	69.2	41.7	72.3	61.3
Nb (ppm)	15.1	13.1	13.2	9.66	11.2	13.2	13.8	12.6	9.74	9.09	10.6	14.8	11.2	9.89	8.91	8.38	5.58	8.89	7.34
Mo (ppm)	4.02	1.51	1.45	1.12	1.35	1.22	0.79	1.07	1.06	0.95	1.91	1.66	1.09	1.17	1.22	13.7	1.25	1.01	0.85
Cd (ppm)	0.14	0.09	0.09	0.04	0.11	0.46	0.75	0.20	0.14	0.12	0.06	0.10	0.11	0.05	0.13	0.07	1.06	0.26	0.26
Cs (ppm)	11.0	9.96	10.3	4.65	6.01	63.4	27.5	19.8	5.10	2.82	228	207	5.90	14.2	308	45	14.0	7.63	9.22
Ba (ppm)	615	434	518	559	545	403	460	505	566	572	437	446	588	513	665	587	508	588	615
La (ppm)	45.8	30.7	32.1	22.7	26.6	30.2	31.6	28.5	22.2	20.3	24.7	35.4	26.2	23.8	20.9	18.5	12.7	21.0	16.4
Ce (ppm)	75.5	60.4	64.0	45.0	53.2	59.9	62.4	57.0	43.7	37.8	48.9	71.1	51.7	47.4	38.2	33.9	23.7	39.0	30.7
Pr (ppm)	10.63	7.00	7.31	5.13	6.04	6.91	7.26	6.59	5.08	4.65	5.59	8.14	5.99	5.46	4.73	4.22	2.86	4.79	3.74
Nd (ppm)	39.3	26.0	27.0	19.1	22.2	25.6	26.7	24.5	19.0	17.4	20.7	30.0	22.3	20.2	17.8	15.9	10.9	17.9	14.1
Sm (ppm)	7.24	4.78	4.94	3.51	4.07	4.71	4.95	4.46	3.54	3.22	3.81	5.50	4.13	3.69	3.30	3.00	2.09	3.26	2.62
Eu (ppm)	1.41	0.94	0.97	0.70	0.81	0.92	0.98	0.89	0.71	0.64	0.76	1.07	0.83	0.74	0.68	0.62	0.45	0.69	0.55
Gd (ppm)	6.16	4.14	4.25	3.09	3.60	4.11	4.36	3.94	3.11	2.82	3.33	4.73	3.69	3.26	2.95	2.69	1.90	2.87	2.37
Tb (ppm)	0.97	0.63	0.64	0.46	0.54	0.63	0.66	0.61	0.47	0.43	0.51	0.73	0.55	0.50	0.45	0.42	0.29	0.45	0.36
Dy (ppm)	5.47	3.70	3.73	2.70	3.10	3.65	3.81	3.52	2.73	2.54	2.92	4.19	3.23	2.86	2.62	2.48	1.79	2.63	2.15
Ho (ppm)	1.09	0.74	0.73	0.53	0.62	0.73	0.77	0.71	0.56	0.51	0.59	0.85	0.65	0.58	0.54	0.51	0.37	0.55	0.45
Er (ppm)	3.01	2.03	2.06	1.50	1.73	2.03	2.16	1.99	1.55	1.46	1.63	2.33	1.80	1.62	1.50	1.42	1.04	1.57	1.29
Tm (ppm)	0.47	0.32	0.31	0.23	0.27	0.32	0.34	0.31	0.24	0.22	0.26	0.36	0.28	0.25	0.24	0.22	0.16	0.25	0.20
Yb (ppm)	2.97	2.01	1.96	1.43	1.65	1.98	2.07	1.92	1.51	1.40	1.60	2.25	1.78	1.56	1.48	1.41	1.00	1.57	1.24
Lu (ppm)	0.44	0.30	0.30	0.22	0.25	0.30	0.32	0.29	0.23	0.21	0.24	0.34	0.27	0.24	0.23	0.21	0.16	0.24	0.19
Hf (ppm)	3.52	2.98	2.86	2.02	2.39	3.18	3.40	3.06	2.22	2.07	2.31	3.40	2.58	2.26	2.10	2.05	1.15	2.18	1.75
Ta (ppm)	1.25	1.01	1.06	0.73	0.86	1.03	1.08	0.97	0.73	0.66	0.88	1.19	0.86	0.75	0.64	0.60	0.36	0.63	0.50

Table 2
(continued)

Sample ID	SCS-NW-1	SCS-NW-2	SCS-NW-3	SCS-NW-4	SCS-NW-5	SCS-NW-6	SCS-NW-7	SCS-NW-8	SCS-NW-9	SCS-NW 10	SCS-NW 11	SCS-NW 12	SCS-NW 13	SCS-NW 14	SCS-NW 15	SCS-NW 16	SCS-N-03-1	SCS-N-03-2	SCS-N-03-3
W (ppm)	2.40	1.83	1.92	1.40	1.66	1.90	1.90	1.80	1.45	1.22	1.57	2.14	1.65	1.48	1.21	1.35	0.65	3.53	0.94
Pb (ppm)	26.3	14.0	17.6	4.90	7.00	11.9	12.3	9.29	4.73	9.28	5.68	12.5	9.22	5.40	4.13	5.73	44.4	31.6	26.5
Th (ppm)	19.1	12.9	13.6	9.41	11.1	12.6	12.6	11.70	8.81	7.88	9.96	14.7	10.5	9.64	7.82	6.83	4.20	7.70	5.85
U (ppm)	3.00	2.25	2.49	2.12	2.28	2.25	2.36	2.35	2.00	1.77	1.94	2.57	2.20	2.07	1.90	1.99	1.34	1.78	1.51

$^{91}Zr/^{90}Zr$ was used to correct instrumental drift (H. C. Liu et al., 2012; Yang et al., 2008). The mass bias of traditional $^{87}Sr/^{86}Sr$ was calibrated using the constant $^{88}Sr/^{86}Sr$ = 8.375209, and that of $\delta^{88}Sr$ was calibrated using the measured $^{88}Sr/^{86}Sr$ of the two adjacent SRM 987 standards. Further details of the measurement are provided by Ma et al. (2013a). The internal precision was better than $\pm 5 \times 10^{-7}$ (1σ) and ±0.01 (1σ) for $^{87}Sr/^{86}Sr$ and $\delta^{88}Sr$, respectively. Standard materials, such as International Association for the Physical Sciences of the Ocean seawater and BCR-2 basalt, were repeatedly chemically treated and measured along with the samples, yielding results of 0.388 ± 0.020 (2SD, n = 6) and 0.231 ± 0.010 (2SD, n = 3) for International Association for the Physical Sciences of the Ocean seawater and BCR-2 basalt, respectively.

The standard sample bracketing mode was also adopted for Nd isotope measurements in the sequence of JNdi-1–sample–JNdi-1. The traditional $^{143}Nd/^{144}Nd$ was obtained by calibrating the mass bias with the constant $^{146}Nd/^{144}Nd = 0.7219$; $\varepsilon^{146}Nd$ was calibrated using the measured $^{146}Nd/^{144}Nd$ of the two adjacent JNdi-1 standards. Details of the method are provided by Ma et al. (2013b). The internal precision was better than $\pm 5 \times 10^{-7}$ (1σ) and ±0.2 (1σ) for $^{143}Nd/^{144}Nd$ and $\varepsilon^{146}Nd$, respectively. Two standard solutions, La Jolla and Nd-GIG, were repeatedly chemically treated and measured along with the samples, yielding $^{143}Nd/^{144}Nd$ and $\varepsilon^{146}Nd$ values of 0.511852 ± 2 and −2.17 ± 0.11 (1SD, n = 3) for La Jolla, and 0.511519 ± 5 and 2.58 ± 0.18 (1SD, n = 4) for Nd-GIG, respectively.

3.3. Lithogenic and Biogenic Matter Estimation

Assuming that Al is mainly associated with lithogenic matter and that the chemical composition of lithogenic matter is similar to the continental crust average values, a standard calculation is used to estimate the lithogenic matter (Hwang et al., 2017; Martinez et al., 2007; Torres Valdés et al., 2014). In this article, Ti is chosen as the normalization element because nonlithogenic Al might exist by biogenic and authigenic processes in the SCS (Wei et al., 2003); and the continental crust average values are represented by Post-Archean Average Shale (PAAS) (Taylor & McLennan, 1985). Subsequently, the concentration of biogenic matter can be calculated from the concentration in the bulk particles by subtracting the contribution of lithogenic matter. Then we have equation

$$M_{lithogenic} = Ti_{bulk} \times (M/Ti)_{PAAS}\ M_{biogenic} = M_{bulk} - M_{lithogenic}$$

where M refers a specific element. As our samples were digested using HF acid, SiO_2 could not be measured directly. The SiO_2 concentration of the bulk particles is determined by $100 - (Al_2O_3 + CaO + Fe_2O_3 + K_2O + MgO + MnO + Na_2O + P_2O_5 + TiO_2)$. The error of SiO_2 values calculated from this formula should be estimated as ~ 3% according to Gaussian error transport equation. The corresponding flux of a specific lithogenic or biogenic element can be calculated by multiplying concentration of the element by the total flux.

4. Results

4.1. Major and Trace Elements

The major and trace element contents of the sinking particles collected by the SCS-NW and SCS-N-03 traps are listed in Tables 1 and 2. As shown in the tables, Al_2O_3 and CaO are the most abundant components, with contents of 6.76–18.27 wt % and 7.88–20.02 wt%, respectively. Strong positive correlations ($r > 0.9$) among Ti and Al, K, Sc, Th, Zr, REEs, and so forth, are observed in Table S1 in the supporting information, indicating that these elements are involved with lithogenic matter. Elements related to biogenic matter have negative correlations with detrital elements. For example, the strong negative correlations ($r < -0.8$) occur between Ca, Sr, and Ti. Compared with Ti, Al has a weaker negative correlation ($r = -0.67$) with Ca, which indicates that Ti is more suitable to represent lithogenic components.

4.2. Sr and Nd Isotopes

The results of Sr and Nd isotopes are listed in Table 3. The $^{87}Sr/^{86}Sr$ values range from 0.709522 to 0.711584, which are typical values for mixed terrestrial detritus (>0.711) and biogenic carbonate (~0.7092). The $^{87}Sr/^{86}Sr$ values of the particles collected by the SCS-NW trap (0.709957–0.711732, with a mean value of 0.710758) are generally higher than those of SCS-N-03 (0.709522–0.709965, with a mean value of

Table 3
Sr and Nd Isotopes of the Sinking Particles Collected by the SCS-NW and SCS-N-03 Traps

Sample ID	$^{87}Sr/^{86}Sr$	$\delta^{88}Sr$	$^{143}Nd/^{144}Nd$	$\varepsilon^{146}Nd$	$\varepsilon^{143}Nd$[a]
SCS-NW-1	0.711265 ± 6	0.234 ± 0.011	0.512103 ± 4	−0.51 ± 0.07	−10.4
SCS-NW-2	0.711584 ± 6	0.215 ± 0.011	0.512112 ± 4	−0.52 ± 0.06	−10.3
SCS-NW-3	0.711546 ± 7	0.197 ± 0.011	0.512144 ± 8	−0.83 ± 0.08	−9.6
SCS-NW-4	0.710540 ± 7	0.213 ± 0.013	0.512108 ± 8	−0.51 ± 0.11	−10.3
SCS-NW-5	0.710798 ± 7	0.194 ± 0.013	0.512116 ± 7	−0.56 ± 0.11	−10.2
SCS-NW-6	0.711397 ± 7	0.215 ± 0.015	0.512098 ± 6	−0.21 ± 0.07	−10.5
SCS-NW-7	0.711203 ± 7	0.247 ± 0.015	0.512094 ± 7	−0.45 ± 0.11	−10.6
SCS-NW-8	0.710775 ± 7	0.236 ± 0.014	0.512117 ± 9	-	−10.2
SCS-NW-9	0.710164 ± 7	0.222 ± 0.015	0.512091 ± 6	−0.46 ± 0.09	−10.7
SCS-NW-10	0.709998 ± 7	0.206 ± 0.016	0.512112 ± 6	−0.44 ± 0.08	−10.3
SCS-NW-11	0.710406 ± 8	0.250 ± 0.014	0.512108 ± 6	−0.11 ± 0.08	−10.3
SCS-NW-12	0.711732 ± 8	0.284 ± 0.015	0.512109 ± 9	−0.67 ± 0.11	−10.3
SCS-NW-13	0.710405 ± 8	0.211 ± 0.016	0.512106 ± 4	−0.24 ± 0.07	−10.4
SCS-NW-14	0.710348 ± 8	0.215 ± 0.015	0.512106 ± 5	−0.31 ± 0.11	−10.4
SCS-NW-15	0.709957 ± 6	0.251 ± 0.014	0.512120 ± 7	−0.43 ± 0.15	−10.1
SCS-NW-16	0.710006 ± 7	0.252 ± 0.015	0.512125 ± 8	−0.67 ± 0.09	−10.0
SCS-N-03-1	0.709522 ± 8	0.234 ± 0.017	0.512118 ± 8	−0.74 ± 0.13	−10.1
SCS-N-03-2	0.709965 ± 8	0.158 ± 0.015	0.512112 ± 8	−1.17 ± 0.17	−10.3
SCS-N-03-3	0.709799 ± 7	0.160 ± 0.014	0.512111 ± 8	−1.23 ± 0.13	−10.3

[a] $\varepsilon^{143}Nd = 10000 \times (^{143}Nd/^{144}Nd/0.512638\text{-}1)$.

0.709762). The $\delta^{88}Sr$ values show a very narrow range, 0.194‰–0.284‰ (mean 0.228‰) for the SCS-NW trap and 0.158‰–0.234‰ (mean 0.184‰) for the SCS-N-03 trap (Table 3). Similar to $^{87}Sr/^{86}Sr$, the $\delta^{88}Sr$ values of the SCS-NW particles are slightly higher than those of the SCS-N-03 particles. The radiogenic Nd isotopes show nearly identical values, with $^{143}Nd/^{144}Nd$ of 0.512091 to 0.512144 and $\varepsilon^{143}Nd$ of −10.7 to −9.6, where $\varepsilon^{143}Nd$ is the traditional radiogenic Nd isotope εNd, defined as 10,000 × ($^{143}Nd/^{144}Nd$/0.512638–1). Herein, we express $\varepsilon^{143}Nd$ in this manner for consistency with the stable Nd isotope $\varepsilon^{146}Nd$. The stable Nd isotope values show similar variations, with $\varepsilon^{146}Nd$ ranging from −1.23 to −0.11.

5. Discussion

5.1. Fluxes and Concentrations of Sinking Particles

The trap SCS-NW is adjacent to the northern continental shelf in the SCS; its temporal variations in TPF, as well as fluxes and concentrations of lithogenic matter (represented by Ti), biogenic carbonate ($CaCO_3$*), and biogenic silica (SiO_2*) are illustrated in Figure 2. The TPF of trap XS1 at 1,500-m water depth varied from 68 to 1,527 mg/m^2/day (J. G. Liu et al., 2014). Similarly, the TPF of SCS-NW at 1,548-m water depth ranged from 120 to 2,500 mg/m^2/day. Two peaks arose during August and October 2012, and the highest peak was observed in February 2013. The fluxes of Ti, $CaCO_3$*, and SiO_2* showed a synchronous trend with TPF, and Ti concentration was also coupled with TPF or Ti flux, but concentrations of $CaCO_3$* and SiO_2* displayed inverse trends with TPF or their fluxes. The features shown in Figure 2 indicate that the captured particles in TPF peaks contain more lithogenic materials than biogenic materials so that the input of these particles decrease the proportion of biogenic materials, and the opposite situation occurred in TPF valleys. The abrupt increase of fluxes between lithogenic and biogenic components during a short interval (15 to 30 days) is a universal characteristic of deep traps and is speculated to be due to lateral transport of resuspended sediments from neighboring shelves (Bonnin et al., 2002; Honda et al., 2000; Hwang et al., 2009, 2017; J. G. Liu et al., 2014). Furthermore, resuspended particles contain low biogenic materials because resuspension can increase the transportation distances of particles and the residence time of carbonate and silicate to undersaturated seawater (Gardner et al., 1985). Thus, the pulses of TPF in SCS-NW trap probably arise from the addition of resuspended particles with high lithogenic materials.

5.2. Estimation on Contribution of Resuspended Sediments

Resuspended materials originate from surface sediments on the seafloor, which consists of lithogenic materials and biogenic materials. As a result, lateral transport of resuspended sediments can result in concomitant

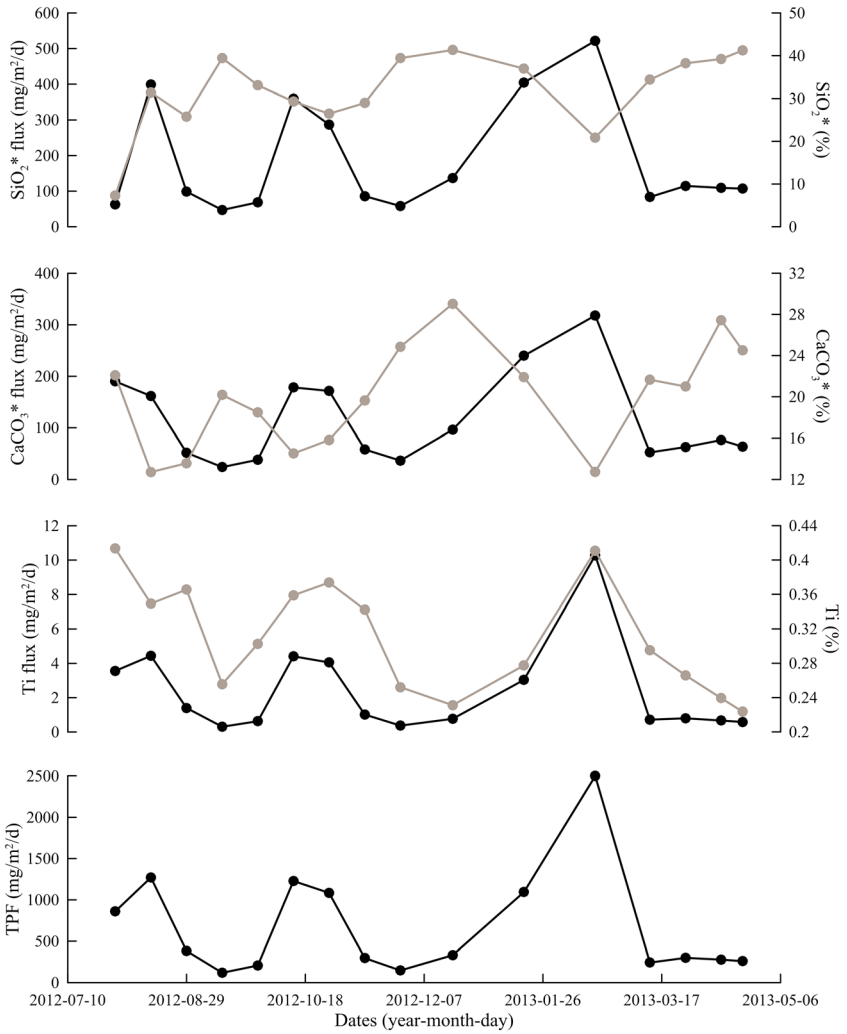

Figure 2. Temporal variations of the SCS-NW in total particle flux (TPF), and in fluxes and concentrations of terrigenous matter (represented by Ti), biogenic carbonate ($CaCO_3$*), and biogenic silicate (SiO_2*); the fluxes and concentrations are indicated by black lines and gray lines, respectively.

pulse between lithogenic materials and biogenic materials, such as descriptions in section 5.1. The fluxes of elements closely related to lithogenic materials usually reflect the enlargement of resuspended sediments, For example, Al is frequently chosen to trace resuspended sediments (Gardner et al., 1985; Hwang et al., 2009, 2017). Similar in section 3.3, excess Al in the SCS makes us employ Ti to mark lithogenic materials.

A positive correlation was shown in diagram of $CaCO_3$ flux versus Al flux at the deep trap, and the intercept of the diagram was employed to evaluate an average $CaCO_3$ flux from vertical sinking and subsequently infer the resuspended fraction of $CaCO_3$ (Hwang et al., 2017). Similarly, Figure 3a exhibits positive correlations between total $CaCO_3$ flux, biogenic $CaCO_3$ ($CaCO_3$*) flux, and Ti flux. It is intriguing that the two linear regression lines in Figure 3a have the same intercept (44.8 mg/m^2/day), which means that the sinking $CaCO_3$ is primarily contributed by calcareous organisms living in overlying water column. The average $CaCO_3$ flux (44.8 mg/m^2/day) from vertical sinking accounts for 36.5% of the total $CaCO_3$ flux on average (122.8 mg/m^2/day), indicating that the $CaCO_3$ of 63.5% may be attributed to resuspended sediments. Both total SiO_2 flux and biogenic SiO_2 (SiO_2*) are positively correlated to Ti flux (Figure 3c), and the two linear regression lines also share the same intercept, 67.5 mg/m^2/day. The average flux (67.5 mg/m^2/day) of sinking SiO_2 produced by siliceous organisms account for 15.8% of the total SiO_2 flux on average (426.7 mg/m^2/day) and 36.7% of the total SiO_2* flux on average (184.1 mg/m^2/day), in other words, 84.2% of total SiO_2 and 63.3% of total SiO_2* may be supplied via lateral transport.

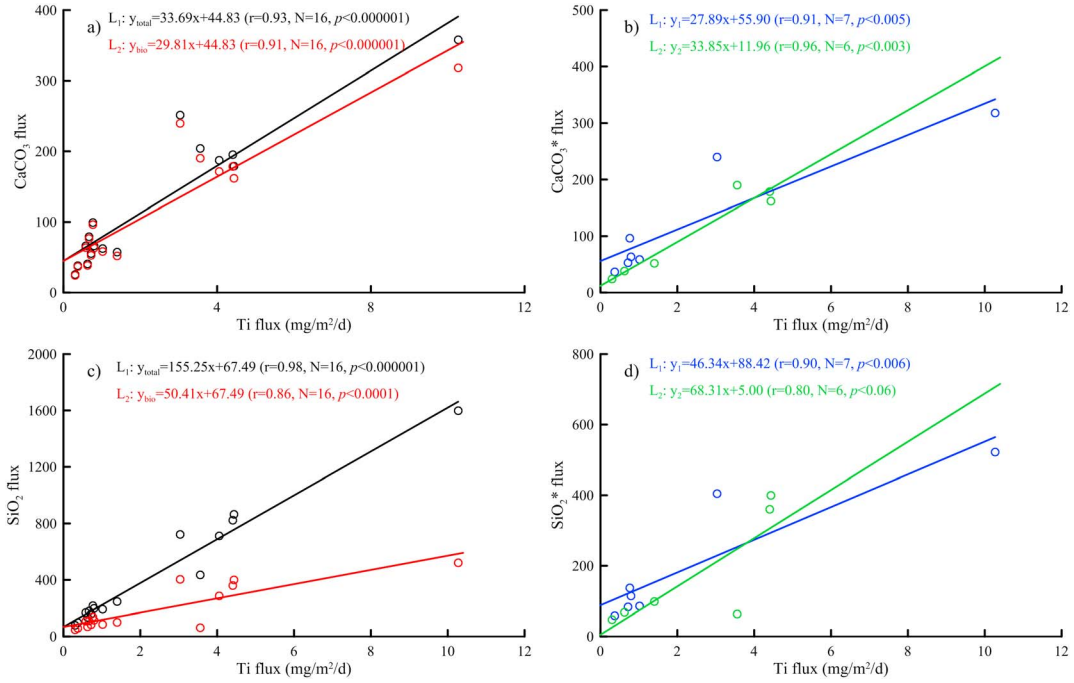

Figure 3. Correlations between total fluxes ($CaCO_3$ and SiO_2), biogenic fluxes ($CaCO_3$* and SiO_2*), and Ti flux for the SCS-NW. The black and red symbols in Figures 3a and 3c represent total fluxes and biogenic fluxes, respectively. In Figures 3b and 3d, winter samples (November to next March) are colored by green and summer samples (May to September) are colored by blue.

As described in section 2, large fluvial sediments are annually transported to the SCS. In addition to resuspended lithogenic materials, terrestrial lithogenic materials may be the other important contributor of trapped sediments in the SCS. Thus, instead of assuming lithogenic materials to be completely provided by resuspended sediments (Hwang et al., 2017), we attempt to estimate terrestrial lithogenic materials by assuming that sinking particles collected by deep trap are derived from the shallow trap. Although we have no data about TPF of the shallow trap with the same sampling location, an alternative shallow trap (sediment trap XS1) near our sampling site can be selected. The average TPF of the shallow trap XS1 is 111 mg/m^2/day (J. G. Liu et al., 2014), associated with the estimated value (112.3 mg/m^2/day) for sinking $CaCO_3$* and SiO_2* collected by the SCS-NW trap, so we can conclude that the lithogenic materials are largely from resuspended sediments.

The relationship between $CaCO_3$* flux and Ti flux during summer and winter is plotted in Figure 3b, which signifies that the average $CaCO_3$* flux in winter is larger than that in summer. Also, as shown in Figure 3d, more SiO_2* flux is observed in winter. The rising flux of biogenic materials, $CaCO_3$* and SiO_2*, is an indication for calcareous and siliceous phytoplankton species blooms in winter. Previous works also have demonstrated that chlorophyll concentration and primary production is higher during winter in the SCS (Chen et al., 2006; Ning et al., 2004; Tan & Shi, 2009). More details about the mechnism for this phenomenon will be discussed in section 5.5.

5.3. Particle Provenance

The sinking particles collected by the traps represent the sediments transported to this region at the present day, and information on the sources of sediment particles provides direct evidence for sediment provenance. As immobile-element discrimination diagrams can be used to identify the sources of sediments in the SCS (Schröder, 2015; Wei et al., 2012), herein we plot La-Th-Sc, Th-Sc-Zr/10, $LREE_{PAAS}/HREE_{PAAS}$-Eu*, and Zr/Sc-Eu* discrimination diagrams for the sinking particles and surface sediments (Figure 4). Among these elemental indices, the subscript PAAS signifies elements are normalized by PAAS, and LREE and HREE represent the sum of La to Eu and that of Gd to Lu, respectively, and Eu* = $2Eu_{(PASS)}/[Sm_{(PAAS)} + Gd_{(PAAS)}]$. In La-Th-Sc

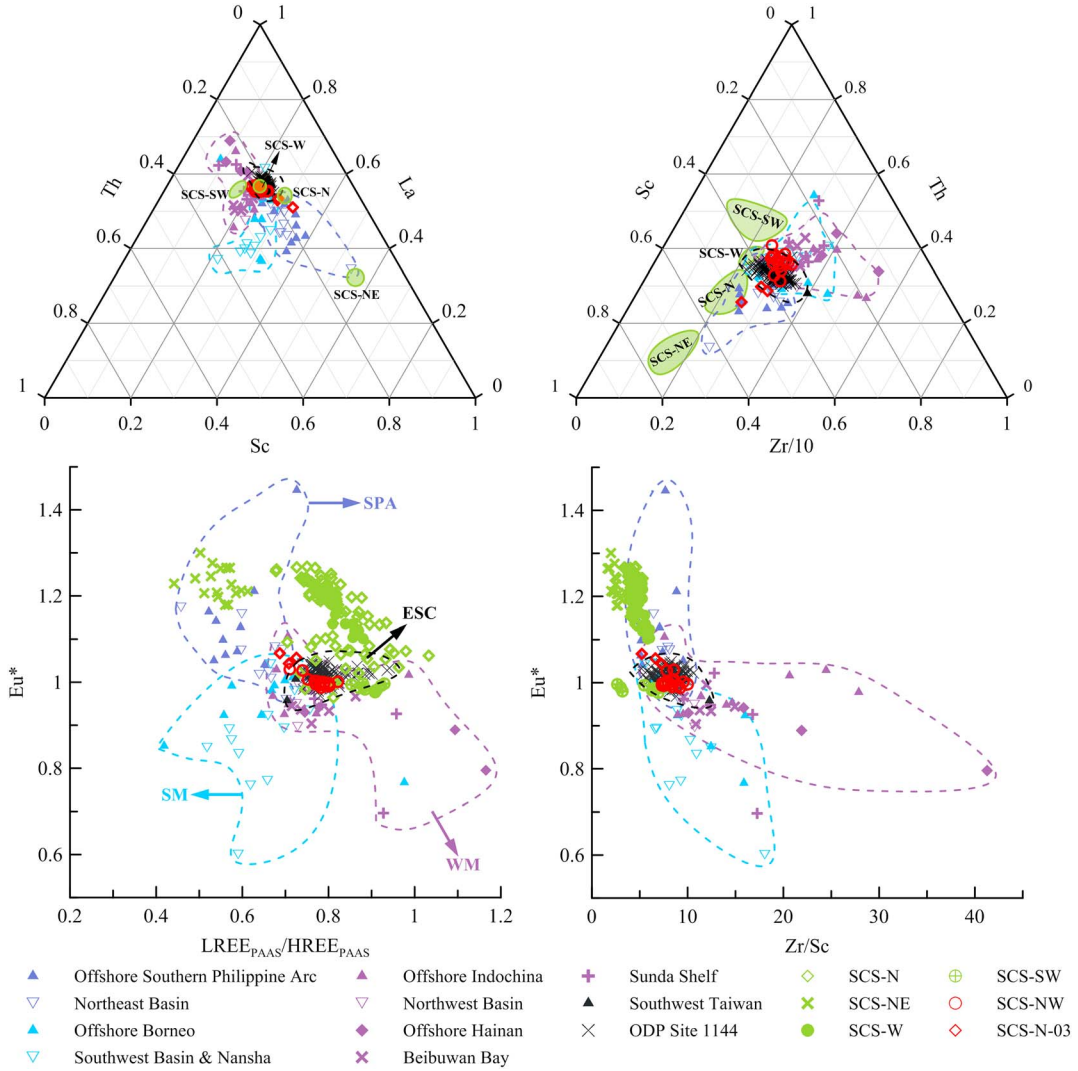

Figure 4. The ternary and binary element discrimination diagrams of sinking particles and surface sediments. The sinking particles of the SCS-NW and SCS-N-03 in this article are represented by red symbols. Green symbols indicate the sinking particles of Schröder (2015); symbols in binary diagrams are plotted using data in the dissertation; the amounts of green diamond in $LREE_{PAAS}/HREE_{PAAS}$-Eu* diagram are more than in Zr/Sc-Eu* diagram because some Zr/Sc ratios of the SCS-N are absent; green polygons in Th-Sc-Zr/10 diagram are depicted based on Figure 33 in the dissertation, and corresponding polygons in La-Th-Sc are inferred associated with Figure 33 and La concentrations in Schröder (2015). Western margin (WM, purple polygon), eastern South China (ESC, black polygon), southern margin (SM, light blue polygon), and Southern Philippine Arc (SPA, royal blue polygon) are the main source regions for the sediments of the SCS. The source regions are identified from the trace elements of the surface sediments (Gao, 2005; Wei et al., 2012) and sediments at ODP site 1144 (Wei et al., 2004), detailed data are in Table S2. ODP = Ocean Drilling Program; LREE = light rare earth element; HREE = heavy rare earth element; PAAS = Post-Archean Average Shale.

diagram, Wei et al. (2012) have characterized regional distribution of offshore surface sediments near ESC, western margin (WM) and southern margin (SM) of the SCS, and southern Philippine Arc (SPA). Except for large overlap between WM and SM in Th-Sc-Zr/10 diagram, distinctively regional distribution of surface sediments also exists in Th-Sc-Zr/10, $LREE_{PAAS}/HREE_{PAAS}$-Eu*, and Zr/Sc-Eu* diagrams. To put in more details, the SPA has high Sc concentration, the most positive Eu* value, low La or LREE concentration, and low Zr concentration; contrary to the SPA, the SM is featured by lower Sc concentration, negative Eu anomaly, and higher Zr concentration; the WM has lowest Sc concentration, negative Eu anomaly, the most La concentration or $LREE_{PAAS}/HREE_{PAAS}$, and the most Zr concentration; the ESC shows intermediate values on abovementioned parameters.

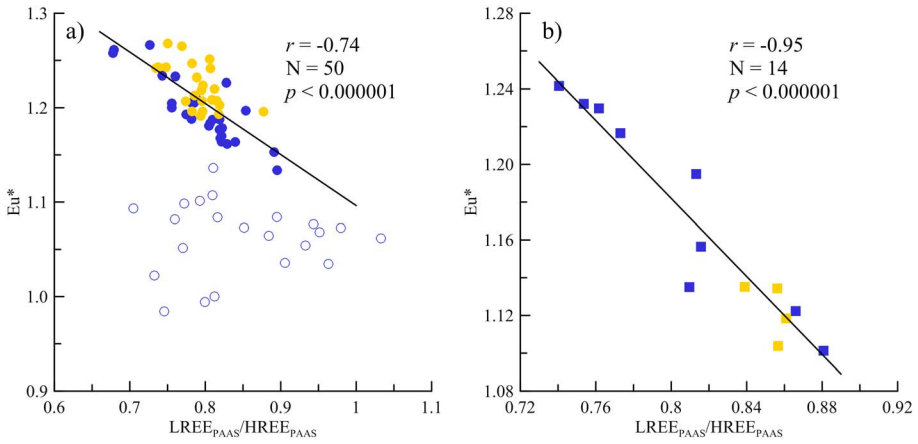

Figure 5. The $LREE_{PAAS}/HREE_{PAAS}$-Eu* discrimination diagram about sinking particles of the SCS-N and SCS-W, in which data are from Schröder (2015). Samples from the SCS-N and SCS-W are symbolled by circles and squares, respectively. The deep blue (yellow) represents samples collected during winter (summer) monsoon. (a) Solid circles denote the samples collected by SCS-N from July 2009 to April 2012, which are also used to draw the regression line; the remains are samples collected from September 1987 to October 1988. (b) These samples were collected by SCS-W from June 2011 to April 2012. LREE = light rare earth element; HREE = heavy rare earth element; PAAS = Post-Archean Average Shale.

Similar to surface sediments, the sinking particles from different regions also show distinctive distributions in the discrimination diagrams (Figure 4). The location of SCS-NE trap (Schröder, 2015) is very close to Luzon Island, which leads its sinking particles and surface sediments from SPA area to sharing similarly elemental patterns in these discrimination diagrams. The sinking particles of SCS-SW trap (Schröder, 2015) nearby Vietnamese coast mainly fall in the WM area in La-Th-Sc, $LREE_{PAAS}/HREE_{PAAS}$-Eu*, and Zr/Sc-Eu* diagrams. Owing to proximity to the coast, selective settling and material mixing weakly impact on offshore sediments so that the particles collected by the SCS-NE and SCS-SW also have geochemical similarity with fluvial sediments from Luzon Rivers and Vietnamese Rivers (Schröder, 2015). Meanwhile, the peak values of TPF on SCS-NE and SCS-SW sometimes coincide between different water depths and the TPF is more in deep depth than in shallow depth (Lahajnar et al., 2007; Schröder, 2015), which means that resuspended sediments from deep water sometimes can be transported upwardly into shallow water. Here we are incapable of assessing the contributions from fluvial sediments and resuspended sediments, but trace elements and TPF of particles collected by offshore traps indicate that resuspended sediments are also an important source of sinking particles near the coast.

The SCS-NW trap is moored in the western of the SCS, close to the Xisha Islands, but its particles are not clearly plotted in the WM and mainly overlap between WM and ESC in the discrimination diagrams. The elemental distribution patterns of the SCS-NW particles indicate that even though transport distances from ESC to Xisha Islands are so long, the sediments from ESC can reach the western of the SCS by resuspension and westward currents. Clay mineral analyses also make the same conclusion that sediments collected by traps near Xisha Through largely contain Taiwanese sediments transported by the deep water current (J. G. Liu et al., 2014). The discussions in sections 5.1 and 5.2 and the geochemical similarity between the sinking particles of the SCS-NW and surface sediments in ESC confirm the speculation that resuspended sediments from the shelf or slope are a main contributor of the sinking particles (Chung et al., 2004; Lahajnar et al., 2007; J. G. Liu et al., 2014).

The sinking particles of the SCS-N and SCS-W traps (Schröder, 2015) basically fall in the SPA and the overlapping region in ternary discrimination diagrams, respectively, which means that the SCS-N particles mainly originate from sediments of the SPA and the SCS-W particles are from mixing sources. However, it is very interesting that the sinking particles of these two traps obviously have similar two-component mixing trends in binary discrimination diagrams (Figure 4). More details about mixing trends and seasonal changes on samples from the SCS-N and SCS-W traps are shown in Figure 5. The samples collected by the SCS-N from 2009 to 2012 exhibit a negative correlation ($r = -0.74$, $N = 50$, $p < 0.000001$) in $LREE_{PAAS}/HREE_{PAAS}$-Eu* diagram (Figure 5a), which indicates that particles in the SCS-N station are mixed sediments from ESC and SPA during this period. The samples collected by the SCS-N trap in 1987 and 1988 winters have lower Eu* values, which

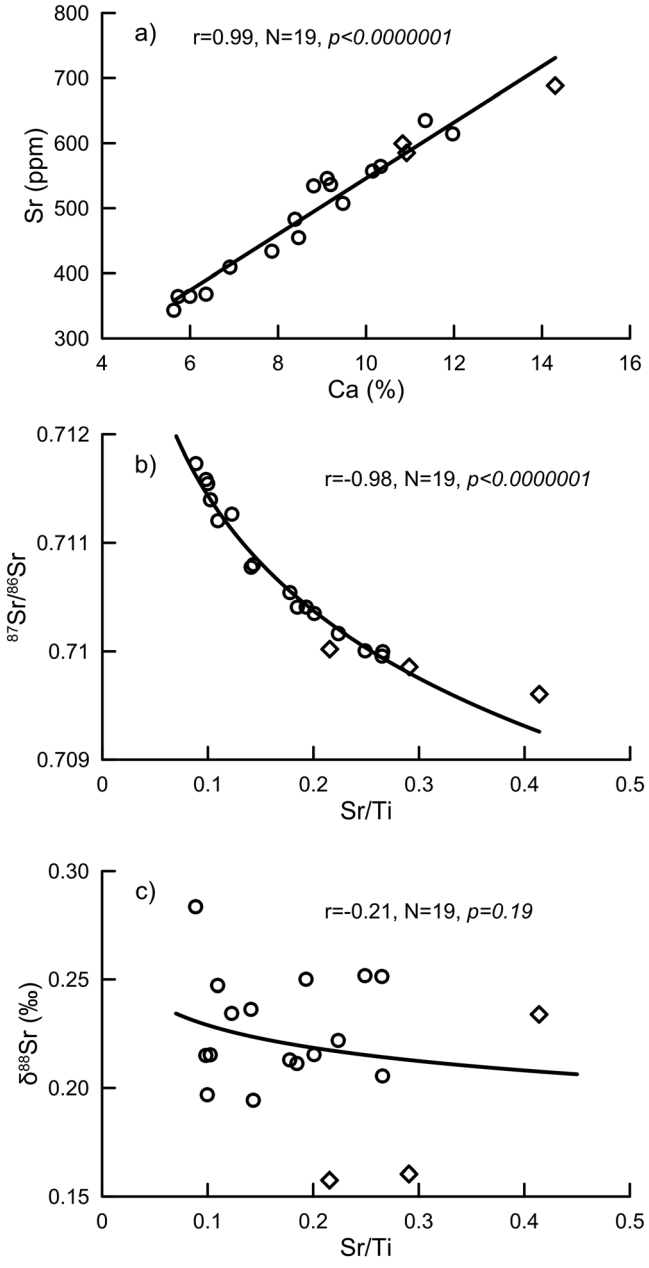

Figure 6. Correlations between (a) Sr and Ca, (b) $^{87}Sr/^{86}Sr$ and Sr/Ti, and (c) $\delta^{88}Sr$ and Sr/Ti for particles from the SCS-NW and SCS-N-03 traps. Open circles mark particles collected by the SCS-NW; open diamonds denote those from the SCS-N-03.

indicates that these particles are mainly derived from ESC in the winter of these 2 years. In the SCS-W station, there is an apparent negative correlation ($r = -0.95$, $N = 14$, $p < 0.000001$) for samples collected during June 2011 to April 2012 (Figure 5b). The winter samples from the SCS-W trap with high Eu* values obviously originate from sediments from SPA and can be laterally transported by deep currents in the southern SCS (Figure 1). The remaining samples with lower Eu* values are mainly from WM because only one westward deep current originated from eastern of the SCS in summer flows through the SCS-W station and possibly carries sediments with high Eu* values from SPA (Figure 1). Moreover, the winter samples have broader range than the summer ones in Figure 5, which reflects that hydrological conditions in winter are more dynamic and variable than in summer.

5.4. Indication of Sr-Nd Isotopes of Sediment Provenance Discrimination

Lithogenic materials and biogenic carbonate are main components of the sinking particles, and Sr is largely concentrated in biogenic carbonate, which is indicated by the robust positive correlation between Sr and Ca (Figure 6a). As biogenic carbonate in modern ocean generally has a high Sr content (Sr/Ti $>$ 1) and low $^{87}Sr/^{86}Sr$ ($<$0.7092, Krabbenhöft et al., 2010), the presence of biogenic carbonate induces a mixed $^{87}Sr/^{86}Sr$ signal of the bulk particles. Figure 6b shows the correlation between $^{87}Sr/^{86}Sr$ and Sr/Ti ratios of the particles, which exhibits a typical mixing line of biogenic carbonate and lithogenic materials (Sr/Ti $<$ 0.1 and $^{87}Sr/^{86}Sr > 0.711$, Wei et al., 2012). The SCS-N-03 particles generally have higher Sr/Ti ratios, indicating a larger amount of biogenic carbonate; as a result, these particles have lower $^{87}Sr/^{86}Sr$ values than those collected by the SCS-NW (Figure 6b). However, unlike the strong correlation between $^{87}Sr/^{86}Sr$ and Sr/Ti ratios, a weak correlation between $\delta^{88}Sr$ and Sr/Ti ratios is shown in Figure 6c, which may imply that $\delta^{88}Sr$ values of lithogenic materials and biogenic carbonate are similar. The similar $\delta^{88}Sr$ values could be caused by fractionations during silicate weathering and biogenic carbonate formation. Most silicate rocks gave $\delta^{88}Sr$ values of 0.2–0.3‰ (Moynier et al., 2010), and chemical weathering could make the residual solids more depleted in ^{88}Sr than parent rocks (Stevenson et al., 2016; Wei et al., 2013). As a result, the residual weathering solids in southwestern Taiwan had $\delta^{88}Sr$ values of 0.08–0.22‰ (Chao et al., 2015). Also, calcareous organisms preferentially take light Sr isotope from seawater ($\delta^{88}Sr = 0.386$‰) so that biogenic marine carbonates possess $\delta^{88}Sr$ values of 0–0.35‰ (Böhm et al., 2012; Krabbenhöft et al., 2010; Y. W. Liu et al., 2015; Stevenson et al., 2014), which largely overlap with those of solid weathering products.

Overall, the variations of radiogenic and stable Sr isotopes of bulk particles not only result from the provenance differences of the particles collected by these two traps but also from the difference in their biogenic carbonate contents. Thus, the presence of biogenic carbonate blurs $^{87}Sr/^{86}Sr$ and $\delta^{88}Sr$ signals of the lithogenic materials, making these parameters invalid for provenance tracing.

Unlike Sr element, the concentration of Nd in biogenic carbonate is generally very low, typically less than 1 μg/g for foraminifer tests collected by tows (Vance et al., 2004), significantly lower than the level in lithogenic materials (20–30 μg/g) in the SCS (Wei et al., 2012). In addition, as a member of REE, Nd has the strong positive correlation ($r = 0.95$) with Ti indicating that it is mainly contributed by lithogenic materials. Thus, the presence of biogenic carbonate does not significantly influence the Nd isotope signal of the lithogenic

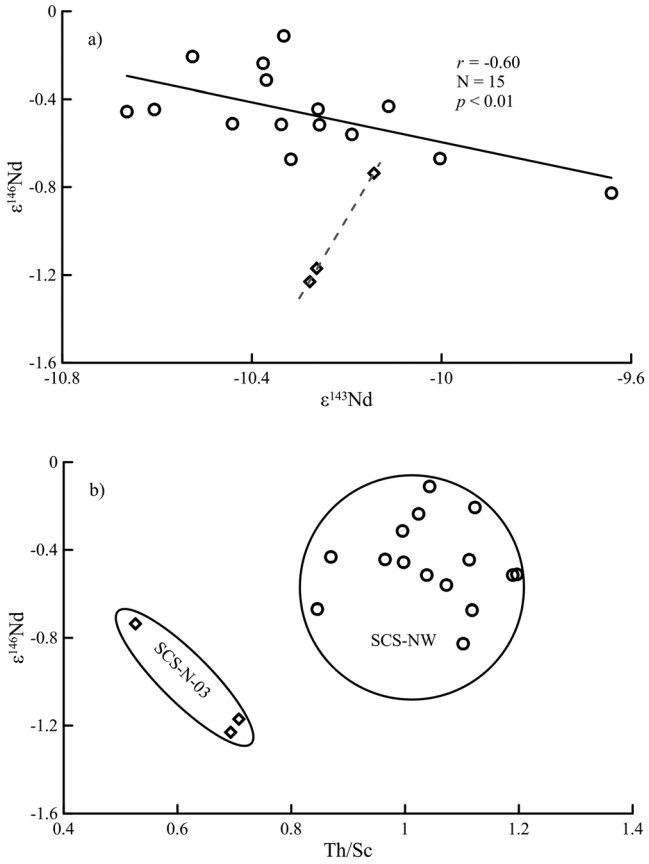

Figure 7. Correlations between (a) ε^{143}Nd and ε^{146}Nd, and (b) Th/Sc and ε^{146}Nd for particles from the two sediment traps. Open circles mark the particles collected by the SCS-NW; open diamonds denote those from the SCS-N-03.

materials in bulk particles, and Nd isotopes could be a reliable indicator of the provenance of the lithogenic materials.

The radiogenic Nd isotope ratio, ^{143}Nd/^{144}Nd, is not sensitive in identifying the provenance of sediments in the northern SCS (Wei et al., 2012), because the ^{143}Nd/^{144}Nd values of the continental terrestrial input from South China and the input from adjacent islands are nearly the same (Z. F. Liu et al., 2007; Shao et al., 2009). This conclusion can also be made from the almost identical ^{143}Nd/^{144}Nd and ε^{143}Nd values of sinking particles collected by the SCS-NW and SCS-N-03 sediment traps (Table 3).

Stable Nd isotopes can provide extra information for identifying the provenance of trapped particles. The particles collected by the SCS-NW trap generally display less negative ε^{146}Nd values, −0.83 to −0.11, whereas those collected by the SCS-N-03 trap have more negative values, −1.23 to −0.74. In addition, the Nd isotopes of the particles collected in the two traps display different trends on the ε^{143}Nd-ε^{146}Nd diagram (Figure 7a). There is an apparent negative correlation ($r = -0.60$, $N = 15$, $p < 0.01$) between ε^{143}Nd and ε^{146}Nd values in the particles of the SCS-NW trap. The SCS-N-03 trap particles probably exhibit a positive correlation between ε^{143}Nd and ε^{146}Nd values, although the significance of this trend could not be estimated because of the small number of data points ($N = 3$). Moreover, the differences in the stable Nd isotopes of the particles from the two traps agree well with those revealed by the elemental discrimination diagrams. Figure 7b shows the correlation between the ε^{146}Nd and Th/Sc ratios. The particles from SCS-NW have higher Th/Sc and ε^{146}Nd values compared with the particles from SCS-N-03. The particles collected by the two traps can therefore be clearly separated. Thus, the use of both stable Nd isotopes and conservative trace elements could potentially identify the provenance of the sediments in the northern SCS.

The time series for the SCS-NW trap covers nearly a whole year, and both the stable Nd isotope and the conservative elements of the trapped particles do not show seasonal variations. Clay mineral assemblages collected by the XS1 trap of the South China Sea Institute of Oceanology, which is located near the SCS-NW trap, also show no seasonal changes (J. G. Liu et al., 2014). No seasonal changes may imply that there is a dominant source for particles supplied to this region or that corresponding sources of these particles share similar geochemistry and clay mineral assemblages. Although seasonal and annual changes of elemental indices are observed in the SCS-N trap (Figure 5a), we cannot discuss the seasonal changes of ε^{146}Nd in this station because our samples of the SCS-N-03 trap are very insufficient.

5.5. Transport Mechanism of Sinking Particles

The characteristics of sinking particles described in sections 5.1 to 5.3 are closely related to hydrodynamic conditions in the SCS, which is primarily controlled by the East Asian Monsoon (section 2). In winter, strong and cold winds blow over the SCS from the northeast, which can stir and cool surface seawater. As a result, surface cooling and wind stirring can deepen mixed layer depth (MLD) in the SCS (Li et al., 2017; Tai et al., 2017; Tseng et al., 2005). Li et al. (2017) had clearly described the significant correlations between MLD and heat flux and wind speed. Enhanced vertical mixing could make nutrients in underlying water layer available for photosynthetic activities in surface water during winter (Tseng et al., 2005). Strong positive correlations between MLD and surface nitrate concentration and net primary production were observed in the central SCS (Li et al., 2017). Therefore, calcareous and siliceous phytoplankton species could bloom in winter so that winter rising fluxes of $CaCO_3$* and SiO_2* were observed in Figure 3d.

Mesoscale eddies are ubiquitous circular motions with high energy and an important nutrient transport mechanism in global ocean; thus, they play a significant role in biological and biogeochemical processes (Goldthwait & Steinberg, 2008; McGillicuddy, 2016; Sweeney et al., 2003). Cyclonic eddy is characterized by

cold water anomalies, elevated isopycnal surfaces, and depressed sea surface and can cause nutrient-enriched upwelling into the euphotic zone. Anticyclonic eddy has characteristics opposite on cyclonic eddy and can cause nutrient-depleted downwelling out of surface sea (McGillicuddy, 2016; Sweeney et al., 2003). Consequently, increased primary production and particle flux can occur in the interior of cyclonic eddy and anticyclonic is not expected to have increases in biological activity (Sweeney et al., 2003). Chlorophyll and export flux enhancements were only observed around the peripheries of anticyclonic eddies, which is possibly caused by submesoscale upwelling along eddy peripheries (McGillicuddy, 2016; Zhou et al., 2013).

As shown in Figure S1, mesoscale eddies can be marked by sea surface height anomaly (SSHA) data obtained from satellite altimetry measurements. Both anticyclonic eddy (SSHA$>$15 cm) and cyclonic eddy (SSHA$<-$15 cm) can be generated in the SCS during summer (May to July 2011) and winter (December 2011 to February 2012), and more cyclonic eddies (anticyclonic eddies) distribute on sea surface of the SCS in winter (summer, Figure S1). Xiu et al. (2010) made a census of eddies in the SCS during 1993–2007 and observed ~32 eddies on average in the SCS each year in which 52% are cyclonic eddies. More eddies can be generated in the SCS during winter because of strong winds and the intrusion of Kuroshio (Xiu et al., 2010). As mentioned in the above paragraph, cyclonic eddies in the SCS are also important nurient contributors to the euphotic zone and can greatly increase primary production and particle flux (Li et al., 2017; Ning et al., 2004; Tan & Shi, 2009; Xiu et al., 2010; Xiu & Chai, 2011). On the contrary, anticyclonic eddies could push water out of the euphotic zone (McGillicuddy, 2016) so that low/depressed biological activities were observed in its interior (Ning et al., 2004; Xiu & Chai, 2011). Thus, more occurrences of cyclonic eddy in the SCS during winter could be another factor responsible for winter increases in chlorophyll concentration and phytoplankton species mentioned in section 5.2.

TPF and trace element concentrations of sinking particles collected by sediment traps become higher with increasing depth in the SCS, which was mainly attributed to lateral transport of resuspended sediments from continental shelves driven by the deep currents (Chung et al., 2004: Lahajnar et al., 2007; J. G. Liu et al., 2014; Schröder, 2015; Schröder et al., 2015). However, there were no mechanisms to explain how these resuspended sediments in deep water layers can be transported upwardly into upper layers, which may cause concomitant pulses of particle flux in different depths, especially for those sediment traps deployed far from continental shelves. As mesoscale eddies are generated in sea surface with their physical, biological, and biogeochemical properties being mostly studied (McGillicuddy, 2016), they may play a very important role in sediment transport in different depths. Some few researches had observed that anticyclonic eddies could export a large amount of sediments from continental shelves into the deep ocean (Washburn et al., 1993; Zhang et al., 2014). Sixfold suspended sediment concentration in deep layer (2,069 m) and low suspended sediment concentration in upper layer (617 m) were observed when anticyclonic eddy passed through (Zhang et al., 2014), which implies that distribution of suspended sediments could be responsive to physical features of anticyclonic eddy. Similarly, cyclonic eddy with upwelling in its interior should carry suspended sediment in deep ocean into upper water layer when lifting nutrient-enriched water mass. For example, TPF pulses were simultaneously observed in shallow (1,000 m), middle (2,160 m), and deep (3,200 m) traps at SCS-N station in June 2011 and February 2012 (Schröder, 2015); these pulses may be attributed to evolutions of cyclonic eddy around the SCS-N station during May to June 2011 and January to February 2012 (Figures S1a, S1b, S1e, and S1f). TPF pulses of SCS-W (1,100 m) were observed in June, July, and December 2011 (Schröder, 2015), when cyclonic eddies were also evolved near the SCS-W station (Figures S1b–S1d). As a consequence, cyclonic eddies may be consider as a conduit for water mass enriched in nutrients and suspended sediments from deep layer to upper layer in the SCS.

Driven by northeast monsoon in winter, a large-scale cyclonic circulation in upper ocean moves around the SCS basin and the intrusion of Kuroshio can significantly affect its north branch (section 2). In addition, many mesoscale eddies could be generated in southwest of Taiwan and west of Luzon and propagate westward along the northern SCS shelf or across the SCS basin, some of them finally arrive at Xisha (G. Wang et al., 2003; Q. Wang et al., 2015). With assistance of westward propagation of cyclonic eddies, sediments with high Eu* value from the Philippine Arc could possibly have an opportunity to get through the SCS basin ($>$4,000 m) and arrive at SCS-W station (1,100 m). These physical ocean processes may enlarge transport ability and distribution area of sediments from the eastern SCS so that sinking particles and surface sediments from other SCS regions partly show elemental geochemistry signature of that from the eastern SCS (Figure 4).

In summary, sediment transport and distribution in the SCS should be controlled by its hydrological conditions mainly driven by the East Asian monsoon. Sediments from continental shelves may be resuspended and transported by deep currents. Mesoscale eddy may be not only responsible for vertical exchange of sediments and nutrients in different water depths but also for episodic transport of large amounts of sediments in the SCS. Enhanced vertical mixing in upper water layer and upwelling driven by cyclonic eddies can increase sediments and nutrients into the euphotic zone, which could result in enhancement of primary production in winter.

6. Conclusions

The Sr and Nd isotopes, as well as major and trace elements of sinking particles collected in the SCS-NW and SCS-N-03 sediment traps moored in the northern SCS, were reported. We investigated the contribution of resuspended sediments and the provenances of these sinking particles by combining our elemental data with published data for sinking particles and surface sediments from the SCS. The availability of Sr and Nd isotopes for bulk sinking particles in provenance analysis was also explored. The main findings are as follows:

1. Resuspended sediments are an important contributor of the sinking particles collected by sediment traps, especially deep traps. In the SCS-NW station, 63.5% of $CaCO_3$ and 84.2% of SiO_2 may be contributed by resuspended sediments, and most of the lithogenic materials are inferentially supplied by resuspension. The average flux of biogenic materials in winter is higher than that in summer.
2. Regional distribution of sinking particles and surface sediments from the SCS is an obvious characteristic in immobile-element discrimination diagrams. The sinking particles and surface sediments near coasts have similar elemental distribution patterns that are comparable to fluvial sediments from corresponding coasts. Those sediment traps deployed far from coasts or near central SCS can collect the particles with elemental signals analogous to surface sediments from shelves, which means resuspended sediments from shelves can be transported over long distances. Samples collected by the SCS-N and SCS-W have two-component mixing trends and seasonal changes in binary discrimination diagrams. The seasonality that winter samples show broader range than summer samples indicates that the sources of winter particles are more variable and hydrological conditions in winter are more dynamic.
3. The $^{87}Sr/^{86}Sr$ and $\delta^{88}Sr$ values of the sinking particles are influenced by the mixing of biogenic carbonate and are not suitable for tracing particle provenance unless given enough sample volume to remove biogenic carbonate.
4. The $^{143}Nd/^{144}Nd$ values of the sinking particles in SCS-NW and SCS-N-03 traps are identical, as are the $\varepsilon^{143}Nd$ values; thus, these parameters are insensitive to particle provenance. The $\varepsilon^{146}Nd$ values of the particles collected by SCS-N-03 trap are more negative than those of SCS-NW trap. More importantly, the particles of the two traps show different correlations between $\varepsilon^{143}Nd$ and $\varepsilon^{146}Nd$. Hence, coupled conservative trace element ratios such as Th/Sc and $\varepsilon^{146}Nd$ can effectively identify the provenance of the sediments in the northern SCS.

Acknowledgments
The authors thank Zhang Le for assistance with the MC-ICP-MS measurements and Deng Wenfeng for suggestions to the structure of the manuscript. The authors would like to thank the Editor S. Bradley Moran and two anonymous reviewers for their helpful comments and constructive suggestions. Aaron Stallard is appreciated for improving the English of the manuscript. This work was financially supported by the National Basic Research Program of China (2016YFA0601204), the National Natural Sciences Foundation of China (41325012 and 41421062), Guangzhou Science Technology and Innovation Commission (201607020008), and the GIG-CAS 135 project 135PY201605. This work is contribution IS-2604 from GIG-CAS. The data for this paper are available as the online supporting data set and from the corresponding author Gangjian Wei (gjwei@gig.ac.cn).

References

Alexander, C. R., Demaster, D. J., & Nittrouer, C. A. (1991). Sediment accumulation in a modern epicontinental-shelf setting: The Yellow Sea. *Marine Geology*, *98*(1), 51–72. https://doi.org/10.1016/0025-3227(91)90035-3

Böhm, F., Eisenhauer, A., Tang, J., Dietzel, M., Krabbenhöft, A., Kisakürek, B., & Horn, C. (2012). Strontium isotope fractionation of planktic foraminifera and inorganic calcite. *Geochimica et Cosmochimica Acta*, *93*, 300–314. https://doi.org/10.1016/j.gca.2012.04.038

Bonnin, J., van Raaphorst, W., Brummer, G. J., van Haren, H., & Malschaert, H. (2002). Intense mid-slope resuspension of particulate matter in the Faeroe-Shetland channel: Short-term deployment of near-bottom sediment traps. *Deep Sea Research Part I: Oceanographic Research Papers*, *49*(8), 1485–1505. https://doi.org/10.1016/s0967-0637(02)00030-4

Boulay, S., Colin, C., Trentesaux, A., Clain, S., Liu, Z., & Lauer-Leredde, C. (2007). Sedimentary responses to the Pleistocene climatic variations recorded in the South China Sea. *Quaternary Research*, *68*(01), 162–172. https://doi.org/10.1016/j.yqres.2007.03.004

Buesseler, K. O., Antia, A. N., Chen, M., Fowler, S. W., Gardner, W. D., Gustafsson, O., et al. (2007). An assessment of the use of sediment traps for estimating upper ocean particle fluxes. *Journal of Marine Research*, *65*(3), 345–416. https://doi.org/10.1357/002224007781567621

Chao, H. C., You, C. F., Liu, H. C., & Chung, C. H. (2015). Evidence for stable Sr isotope fractionation by silicate weathering in a small sedimentary watershed in southwestern Taiwan. *Geochimica et Cosmochimica Acta*, *165*, 324–341. https://doi.org/10.1016/j.gca.2015.06.006

Chen, C. C., Shiah, F. K., Chung, S. W., & Liu, K. K. (2006). Winter phytoplankton blooms in the shallow mixed layer of the South China Sea enhanced by upwelling. *Journal of Marine Systems*, *59*(1–2), 97–110. https://doi.org/10.1016/j.jmarsys.2005.09.002

Chen, J. F., Zheng, L. F., Wiesner, M. G., Chen, R. H., Zheng, Y. L., & Wong, H. K. (1998). Estimations of primary production and export production in the South China Sea based on sediment trap experiments. *Chinese Science Bulletin*, *43*(7), 583–586. https://doi.org/10.1007/Bf02883645

Chung, Y., Chang, H. C., & Hung, G. W. (2004). Particulate flux and ^{210}Pb determined on the sediment trap and core samples from the northern South China Sea. *Continental Shelf Research*, *24*(6), 673–691. https://doi.org/10.1016/j.csr.2004.01.003

Fang, G., Fang, W., Fang, Y., & Wang, K. (1998). A survey of studies on the South China Sea upper ocean circulation. *Acta Oceanographica Taiwanica*, *37*, 1–16.

Gao, Z. Y. (2005). The geochemical characteristics and provenance of the surface sediment in South China Sea, (Doctoral dissertation). Retrieved from Wanfang data. Chengdu, SC: Chengdu University of Technology. http://www.wanfangdata.com.cn/details/detail.do?_type=degree&id=Y844595

Gardner, W. D., Southard, J. B., & Hollister, C. D. (1985). Sedimentation, resuspension and chemistry of particles in the northwest Atlantic. *Marine Geology*, *65*(3–4), 199–242. https://doi.org/10.1016/0025-3227(85)90057-X

Goldstein, S. J., & Jacobsen, S. B. (1988). Nd and Sr isotopic systematics of river water suspended material: Implications for crustal evolution. *Earth and Planetary Science Letters*, *87*(3), 249–265. https://doi.org/10.1016/0012-821x(88)90013-1

Goldstein, S. L., & Hemming, S. R. (2003). Long-lived isotopic tracers in oceanography, paleoceanography, and ice-sheet dynamics. In K. K. Turekian (Ed.), *Treatise on Geochemistry* (pp. 453–489). Oxford: Pergamon. https://doi.org/10.1016/B0-08-043751-6/06179-X

Goldstein, S. L., Onions, R. K., & Hamilton, P. J. (1984). A Sm-Nd isotopic study of atmospheric dusts and particulates from major river systems. *Earth and Planetary Science Letters*, *70*(2), 221–236. https://doi.org/10.1016/0012-821x(84)90007-4

Goldthwait, S. A., & Steinberg, D. K. (2008). Elevated biomass of mesozooplankton and enhanced fecal pellet flux in cyclonic and mode-water eddies in the Sargasso Sea. *Deep Sea Research Part II: Topical Studies in Oceanography*, *55*(10–13), 1360–1377. https://doi.org/10.1016/j.dsr2.2008.01.003

Honda, M. C., Kusakabe, M., Nakabayashi, S., & Katagiri, M. (2000). Radiocarbon of sediment trap samples from the Okinawa trough: Lateral transport of ^{14}C-poor sediment from the continental slope. *Marine Chemistry*, *68*(3), 231–247. https://doi.org/10.1016/s0304-4203(99)00080-8

Hu, J., Kawamura, H., Hong, H., & Qi, Y. (2000). A review on the currents in the South China Sea: Seasonal circulation, South China Sea warm current and Kuroshio intrusion. *Journal of Oceanography*, *56*(6), 607–624. https://doi.org/10.1023/a:1011117531252

Huang, Q. Z., Wang, W. Z., Li, Y. S., & Li, C. W. (1994). Current characteristics of the South China Sea. In D. Zhou, Y. B. Liang, & C. K. Zeng (Eds.), *Oceanology of China Seas* (pp. 39–47). Dordrecht: Springer Netherlands. https://doi.org/10.1007/978-94-011-0862-1_5

Hwang, J., Manganini, S. J., Montlucon, D. B., & Eglinton, T. I. (2009). Dynamics of particle export on the northwest Atlantic margin. *Deep-sea Research Part I-oceanographic Research Papers*, *56*(10), 1792–1803. https://doi.org/10.1016/j.dsr.2009.05.007

Hwang, J., Manganini, S. J., Park, J., Montlucon, D. B., Toole, J. M., & Eglinton, T. I. (2017). Biological and physical controls on the flux and characteristics of sinking particles on the northwest Atlantic margin. *Journal of Geophysical Research: Oceans*, *122*, 4539–4553. https://doi.org/10.1002/2016JC012549

Jiang, F., Zhou, Y., Nan, Q., Zhou, Y., Zheng, X., Li, T., et al. (2016). Contribution of Asian dust and volcanic material to the western Philippine Sea over the last 220 kyr as inferred from grain size and Sr-Nd isotopes. *Journal of Geophysical Research: Oceans*, *121*, 6911–6928. https://doi.org/10.1002/2016JC012000

Krabbenhöft, A., Eisenhauer, A., Böhm, F., Vollstaedt, H., Fietzke, J., Liebetrau, V., et al. (2010). Constraining the marine strontium budget with natural strontium isotope fractionations (^{87}Sr/^{86}Sr*, $\delta^{88/86}$Sr) of carbonates, hydrothermal solutions and river waters. *Geochimica et Cosmochimica Acta*, *74*(14), 4097–4109. https://doi.org/10.1016/j.gca.2010.04.009

Lahajnar, N., Wiesner, M. G., & Gaye, B. (2007). Fluxes of amino acids and hexosamines to the deep South China Sea. *Deep-sea Research Part I-oceanographic Research Papers*, *54*(12), 2120–2144. https://doi.org/10.1016/j.dsr.2007.08.009

Li, H. L., Wiesner, M. G., Chen, J. F., Ling, Z., Zhang, J. J., & Ran, L. H. (2017). Long-term variation of mesopelagic biogenic flux in the central South China Sea: Impact of monsoonal seasonality and mesoscale eddy. *Deep-sea Research Part I-oceanographic Research Papers*, *126*, 62–72. https://doi.org/10.1016/j.dsr.2017.05.012

Li, X. H., Liu, Y., Tu, X. L., Hu, G. Q., & Zeng, W. (2002). Precise determination of chemical compositions in silicate rocks using ICP-AES and ICP-MS: A comparative study of sample digestion techniques of alkali fusion and acid dissolution. *Geochimica*, *167*(9), 550–557. https://doi.org/10.3321/j.issn:0379-1726.2002.03.010

Li, X. H., Wei, G. J., Shao, L., Liu, Y., Liang, X. R., Jian, Z., et al. (2003). Geochemical and Nd isotopic variations in sediments of the South China Sea: A response to Cenozoic tectonism in SE Asia. *Earth and Planetary Science Letters*, *211*(3–4), 207–220. https://doi.org/10.1016/S0012-821x(03)00229-2

Liu, H. C., You, C. F., Huang, K. F., & Chung, C. H. (2012). Precise determination of triple Sr isotopes (δ^{87}Sr and δ^{88}Sr) using MC-ICP-MS. *Talanta*, *88*, 338–344. https://doi.org/10.1016/j.talanta.2011.10.050

Liu, J. G., Clift, P. D., Yan, W., Chen, Z., Chen, H., Xiang, R., & Wang, D. X. (2014). Modern transport and deposition of settling particles in the northern South China Sea: Sediment trap evidence adjacent to Xisha trough. *Deep-sea Research Part I-oceanographic Research Papers*, *93*, 145–155. https://doi.org/10.1016/j.dsr.2014.08.005

Liu, J. G., Xiang, R., Chen, M. H., Chen, Z., Yan, W., & Liu, F. (2011). Influence of the Kuroshio current intrusion on depositional environment in the northern South China Sea: Evidence from surface sediment records. *Marine Geology*, *285*(1–4), 59–68. https://doi.org/10.1016/j.margeo.2011.05.010

Liu, J. G., Xiang, R., Chen, Z., Chen, M. H., Yan, W., Zhang, L. L., & Chen, H. (2013). Sources, transport and deposition of surface sediments from the South China Sea. *Deep-sea Research Part I-oceanographic Research Papers*, *71*, 92–102. https://doi.org/10.1016/j.dsr.2012.09.006

Liu, Y., Liu, H. C., & Li, X. H. (1996). Simultaneous precise determination of 40 trace elements in rock samples using ICP-MS. *Geochimica*, *25*(6), 552–558. https://doi.org/10.3321/j.issn:0379-1726.1996.06.004

Liu, Y. W., Aciego, S. M., & Wanamarker, A. D. (2015). Environmental controls on the boron and strontium isotopic composition of aragonite shell material of cultured *Arctica islandica*. *Biogeosciences*, *12*(11), 3351–3368. https://doi.org/10.5194/bg-12-3351-2015

Liu, Z. F., Colin, C., Huang, W., Le, K. P., Tong, S. Q., Chen, Z., & Trentesaux, A. (2007). Climatic and tectonic controls on weathering in South China and Indochina peninsula: Clay mineralogical and geochemical investigations from the Pearl, Red, and Mekong drainage basins. *Geochemistry, Geophysics, Geosystems*, *8*, Q05005. https://doi.org/10.1029/2006GC001490

Liu, Z. F., Colin, C., Li, X. J., Zhao, Y. L., Tuo, S. T., Chen, Z., et al. (2010). Clay mineral distribution in surface sediments of the northeastern South China Sea and surrounding fluvial drainage basins: Source and transport. *Marine Geology*, *277*(1–4), 48–60. https://doi.org/10.1016/j.margeo.2010.08.010

Liu, Z. F., Tuo, S. T., Colin, C., Liu, J. T., Huang, C. Y., Selvaraj, K., et al. (2008). Detrital fine-grained sediment contribution from Taiwan to the northern South China Sea and its relation to regional ocean circulation. *Marine Geology*, *255*(3–4), 149–155. https://doi.org/10.1016/j.margeo.2008.08.003

Liu, Z. F., Zhao, Y. L., Colin, C., Stattegger, K., Wiesner, M. G., Huh, C. A., et al. (2016). Source-to-sink transport processes of fluvial sediments in the South China Sea. *Earth-Science Reviews*, *153*, 238–273. https://doi.org/10.1016/j.earscirev.2015.08.005

Ma, J. L., Wei, G. J., Liu, Y., Ren, Z. Y., Xu, Y. G., & Yang, Y. H. (2013a). Precise measurement of stable ($\delta^{88/86}$Sr) and radiogenic (^{87}Sr/^{86}Sr) strontium isotope ratios in geological standard reference materials using MC-ICP-MS. *Chinese Science Bulletin*, *58*(25), 3111–3118. https://doi.org/10.1007/s11434-013-5803-5

Ma, J. L., Wei, G. J., Liu, Y., Ren, Z. Y., Xu, Y. G., & Yang, Y. H. (2013b). Precise measurement of stable neodymium isotopes of geological materials by using MC-ICP-MS. *Journal of Analytical Atomic Spectrometry*, *28*(12), 1926–1931. https://doi.org/10.1039/c3ja50229e

Martin, J. M., Zhang, J., Shi, M. C., & Zhou, Q. (1993). Actual flux of the Huanghe (Yellow-River) sediment to the western Pacific-Ocean. *Netherlands Journal of Sea Research*, *31*(3), 243–254. https://doi.org/10.1016/0077-7579(93)90025-N

Martinez, N. C., Murray, R. W., Thunell, R. C., Peterson, L. C., Muller-Karger, F., Astor, Y., & Varela, R. (2007). Modern climate forcing of terrigenous deposition in the tropics (Cariaco Basin, Venezuela). *Earth and Planetary Science Letters*, *264*(3–4), 438–451. https://doi.org/10.1016/j.epsl.2007.10.002

McGillicuddy, D. J. (2016). Mechanisms of physical-biological-biogeochemical interaction at the oceanic mesoscale. *Annual Review of Marine Science*, *8*(1), 125–159. https://doi.org/10.1146/annurev-marine-010814-015606

Milliman, J. D., & Farnsworth, K. L. (2013). *River discharge to the coastal ocean: A global synthesis*. New York, NY: Cambridge University Press.

Milliman, J. D., & Syvitski, J. P. M. (1992). Geomorphic/tectonic control of sediment discharge to the ocean: The importance of small mountainous rivers. *Journal of Geology*, *100*(5), 525–544. https://doi.org/10.1086/629606

Moynier, F., Agranier, A., Hezel, D. C., & Bouvier, A. (2010). Sr stable isotope composition of Earth, the Moon, Mars, Vesta and meteorites. *Earth and Planetary Science Letters*, *300*(3-4), 359–366. https://doi.org/10.1016/j.epsl.2010.10.017

Ning, X., Chai, F., Xue, H., Cai, Y., Liu, C., & Shi, J. (2004). Physical-biological oceanographic coupling influencing phytoplankton and primary production in the South China Sea. *Journal of Geophysical Research*, *109*, C10005. https://doi.org/10.1029/2004JC002365

Qiao, S. Q., Shi, X. F., Wang, G. Q., Zhou, L., Hu, B. Q., Hu, L. M., et al. (2017). Sediment accumulation and budget in the Bohai Sea, Yellow Sea and East China Sea. *Marine Geology*, *390*, 270–281. https://doi.org/10.1016/j.margeo.2017.06.004

Schröder, A. (2015). Changes of clay mineral and trace element characteristics of sinking particulate matter during transport into the Deep South China Sea, (Doctoral dissertation). Retrieved from State and University Library Hamburg. Hamburg: Hamburg University. http://ediss.sub.uni-hamburg.de/volltexte/2016/7805

Schröder, A., Wiesner, M. G., & Liu, Z. F. (2015). Fluxes of clay minerals in the South China Sea. *Earth and Planetary Science Letters*, *430*, 30–42. https://doi.org/10.1016/j.epsl.2015.08.001

Shao, L., Qiao, P. J., Pang, X., Wei, G. J., Li, Q. Y., Miao, W. L., & Li, A. (2009). Nd isotopic variations and its implications in the recent sediments from the northern South China Sea. *Chinese Science Bulletin*, *54*(2), 311–317. https://doi.org/10.1007/s11434-008-0453-8

Shaw, P. T., & Chao, S. Y. (1994). Surface circulation in the South China Sea. *Deep-sea Research Part I-oceanographic Research Papers*, *41*(11–12), 1663–1683. https://doi.org/10.1016/0967-0637(94)90067-1

Stevenson, E. I., Aciego, S. M., Chutcharavan, P., Parkinson, I. J., Burton, K. W., Blakowski, M. A., & Arendt, C. A. (2016). Insights into combined radiogenic and stable strontium isotopes as tracers for weathering processes in subglacial environments. *Chemical Geology*, *429*, 33–43. https://doi.org/10.1016/j.chemgeo.2016.03.008

Stevenson, E. I., Hermoso, M., Rickaby, R. E. M., Tyler, J. J., Minoletti, F., Parkinson, I. J., et al. (2014). Controls on stable strontium isotope fractionation in coccolithophores with implications for the marine Sr cycle. *Geochimica et Cosmochimica Acta*, *128*, 225–235. https://doi.org/10.1016/j.gca.2013.11.043

Sweeney, E. N., McGillicuddy, D. J., & Buesseler, K. O. (2003). Biogeochemical impacts due to mesoscale eddy activity in the Sargasso Sea as measured at the Bermuda Atlantic Time-series Study (BATS). *Deep Sea Research Part II: Topical Studies in Oceanography*, *50*(22–26), 3017–3039. https://doi.org/10.1016/j.dsr2.2003.07.008

Szczucinski, W., Jagodzinski, R., Hanebuth, T. J. J., Stattegger, K., et al. (2013). Modern sedimentation and sediment dispersal pattern on the continental shelf off the Mekong River delta, South China Sea. *Global and Planetary Change*, *110*, 195–213. https://doi.org/10.1016/j.gloplacha.2013.08.019

Tai, J. H., Wong, G. T., & Pan, X. (2017). Upper water structure and mixed layer depth in tropical waters: The SEATS station in the northern South China Sea. *Terrestrial, Atmospheric and Oceanic Sciences*, *28*(6), 1019–1032. https://doi.org/10.3319/TAO.2017.01.09.01

Tan, S. C., & Shi, G. Y. (2009). Spatiotemporal variability of satellite-derived primary production in the South China Sea, 1998–2006. *Journal of Geophysical Research*, *114*, G03015. https://doi.org/10.1029/2008JG000854

Taylor, S. R., & McLennan, S. M. (1985). *The continental crust: Its composition and evolution*. Palo Alto, CA: Blackwell Scientific Publisher.

Torres Valdés, S., Painter, S. C., Martin, A. P., Sanders, R., & Felden, J. (2014). Data compilation of fluxes of sedimenting material from sediment traps in the Atlantic Ocean. *Earth System Science Data*, *6*(1), 123–145. https://doi.org/10.5194/essd-6-123-2014

Tseng, C. M., Wong, G. T., Lin, I. I., Wu, C. R., & Liu, K. K. (2005). A unique seasonal pattern in phytoplankton biomass in low-latitude waters in the South China Sea. *Geophysical Research Letters*, *32*, L08608. https://doi.org/10.1029/2004GL022111

Vance, D., Scrivner, A. E., Beney, P., Staubwasser, M., Henderson, G. M., & Slowey, N. C. (2004). The use of foraminifera as a record of the past neodymium isotope composition of seawater. *Paleoceanography*, *19*, PA2009. https://doi.org/10.1029/2003PA000957

Wang, G., Su, J., & Chu, P. C. (2003). Mesoscale eddies in the South China Sea observed with altimeter data. *Geophysical Research Letters*, *30*(21), 2121. https://doi.org/10.1029/2003GL018532

Wang, Q., Zeng, L., Zhou, W., Xie, Q., Cai, S., Yao, J., & Wang, D. (2015). Mesoscale eddies cases study at Xisha waters in the South China Sea in 2009/2010. *Journal of Geophysical Research: Oceans*, *120*, 517–532. https://doi.org/10.1002/2014JC009814

Wang, S. H., Hsu, N. C., Tsay, S. C., Lin, N. H., Sayer, A. M., Huang, S. J., & Lau, W. K. (2012). Can Asian dust trigger phytoplankton blooms in the oligotrophic northern South China Sea? *Geophysical Research Letters*, *39*, L05811. https://doi.org/10.1029/2011GL050415

Washburn, L., Swenson, M. S., Largier, J. L., Kosro, P. M., & Ramp, S. R. (1993). Cross-shelf sediment transport by an anticyclonic eddy off Northern California. *Science*, *261*(5128), 1560–1564. https://doi.org/10.1126/science.261.5128.1560

Wei, G., Ma, J., Liu, Y., Xie, L., Lu, W., Deng, W., et al. (2013). Seasonal changes in the radiogenic and stable strontium isotopic composition of Xijiang River water: Implications for chemical weathering. *Chemical Geology*, *343*, 67–75. https://doi.org/10.1016/j.chemgeo.2013.02.004

Wei, G. J., Liu, Y., Li, X. H., Chen, M. H., & Wei, W. C. (2003). High-resolution elemental records from the South China Sea and their paleoproductivity implications. *Paleoceanography*, *18*(2), 1054. https://doi.org/10.1029/2002PA000826

Wei, G. J., Liu, Y., Li, X. H., Shao, L., & Fang, D. Y. (2004). Major and trace element variations of the sediments at ODP site 1144, South China Sea, during the last 230 ka and their paleoclimate implications. *Palaeogeography Palaeoclimatology Palaeoecology*, *212*(3–4), 331–342. https://doi.org/10.1016/j.palaeo.2004.06.011

Wei, G. J., Liu, Y., Ma, J. L., Xie, L. H., Chen, J. F., Deng, W. F., & Tang, S. (2012). Nd, Sr isotopes and elemental geochemistry of surface sediments from the South China Sea: Implications for provenance tracing. *Marine Geology*, *319-322*, 21–34. https://doi.org/10.1016/j.margeo.2012.05.007

Xiu, P., & Chai, F. (2011). Modeled biogeochemical responses to mesoscale eddies in the South China Sea. *Journal of Geophysical Research*, *116*, C10006. https://doi.org/10.1029/2010JC006800

Xiu, P., Chai, F., Shi, L., Xue, H. J., & Chao, Y. (2010). A census of eddy activities in the South China Sea during 1993–2007. *Journal of Geophysical Research*, *115*, C03012. https://doi.org/10.1029/2009JC005657

Yan, Q. S., Shi, X. F., & Wang, K. S. (2007). Mineral provinces and material provenance of the surficial sediments near the Zhongsha Islands in the South China Sea. *Acta Oceanologica Sinica*, *26*(1), 66–76.

Yang, L., Peter, C., Panne, U., & Sturgeon, R. E. (2008). Use of Zr for mass bias correction in strontium isotope ratio determinations using MC-ICP-MS. *Journal of Analytical Atomic Spectrometry*, *23*(9), 1269–1274. https://doi.org/10.1039/b803143f

Zhang, Y., Liu, Z., Zhao, Y., Wang, W., Li, J., & Xu, J. (2014). Mesoscale eddies transport deep-sea sediments. *Scientific Reports*, *4*(1), 5937. https://doi.org/10.1038/srep05937

Zhou, K., Dai, M., Kao, S. J., Wang, L., Xiu, P., Chai, F., et al. (2013). Apparent enhancement of ^{234}Th-based particle export associated with anticyclonic eddies. *Earth and Planetary Science Letters*, *381*, 198–209. https://doi.org/10.1016/j.epsl.2013.07.039

Zhu, Y. H., Fang, G. H., Wei, Z. X., Wang, Y. G., Teng, F., & Qu, T. D. (2016). Seasonal variability of the meridional overturning circulation in the South China Sea and its connection with inter-ocean transport based on SODA2.2.4. *Journal of Geophysical Research: Oceans*, *121*, 3090–3105. https://doi.org/10.1002/2015JC011443